Progress Report: Retrieval of Cloud Properties and Aerosol Direct Radiative Forcing

22nd CERES Science Team Meeting
University of Alabama, Huntsville
20-22 September 2000

M.A. Friedman, W.R. Tahnk, and J.A. Coakley, Jr.

College of Oceanic and Atmospheric Science
Oregon State University
Corvallis, OR 97331-5503

Introduction

Work at OSU since the previous Science Team Meeting focused on the following three objectives: 1) causes were sought for the relatively large differences in droplet effective radii retrieved by VINT and by the OSU retrieval scheme for pixels overcast by low-level, single-layered water clouds; 2) the OSU retrieval scheme was extended to obtain properties for fields of view that are only partly cloud covered, and 3) comparisons were made of calculated and observed shortwave radiances for cloud-free ocean scenes in order to pursue estimates of the aerosol direct radiative forcing for cloud-free oceans.

VINT−OSU Comparisons

Differences between the NASA Langley VINT and OSU retrieved droplet effective radii for pixels overcast by single-layered, low-level water clouds are often as high as 5 – 7 μm. Such differences are unreasonable given the similarity and sophistication of the radiative transfer calculations employed in both retrieval schemes. The differences prompted a rigorous re-examination of the OSU retrieval scheme, comparisons of results from the Langley and OSU radiative transfer calculations, and comparisons of VINT and OSU retrieved products at the pixel scale.

The re-examination of the OSU scheme included comparisons of gaseous transmission and emission with the original source code (Kratz 1995) and comparisons of top of the atmosphere radiances for an emitting and scattering atmosphere as calculated by DISORT (Stamnes et al. 1988) with those produced by the parametric scheme used in the retrievals. These comparisons revealed no errors in the OSU radiative transfer calculations and the use of the radiative transfer results in the retrieval scheme.

Two errors were, however, found in the OSU retrieval scheme. First, for some of the retrieved products, the OSU scheme was using an incorrect solar relative azimuth angle. Second, an incorrect value was used for the filter response function in one of the five subchannels of the 3.7-μm band. The effect of these errors are illustrated through comparison of retrieved products with the old (incorrect) and new (corrected) retrieval schemes. The large differences in retrieved 0.63-μm optical depths are due to the use of an incorrect azimuth angle by the old scheme in some of the retrievals. The larger droplet effective radii obtained with the new scheme are the result of the corrected filter response function. Most of the changes in effective radii are due to changes in the calculated thermal emission at 3.7 μm. Calculations of 3.7-μm radiances for clouds with 10-μm droplets reveal that with the emission held fixed at the old value, the effect of the filter function on reflected sunlight produces little change to the radiance.

Checks were made of gaseous absorption calculated with the VINT and OSU radiative transfer codes. Table 1 shows downward transmittances and top of the atmosphere reflectances for McClatchey tropical and midlatitude summer climatological profiles of temperature and humidity. Results are shown for atmospheres over Lambertian surfaces with albedos of 0.2 and 0.7. The OSU code contains more

absorption. It allows for absorption by CH_4 and N_2O not accounted for in VINT. The effect of the extra absorption is to reduce the OSU droplet radii by as much as 2 μm below those of VINT. This difference, however, is too small to account for differences in the retrieved droplet effective radii.

Calculations of top of atmosphere emission for a cloud-free atmosphere over a reflecting and emitting surface were also performed. The emission ($mWm^{-2}sr^{-1}cm$) is given in Table 2. In the calculations, the surface temperature is set to be equal to the temperature of the lowest atmospheric level. The effects of CH_4 and N_2O on the emitted radiances are below the 5% level. Comparisons with Langley will be included as soon as the Langley results become available.

Solar zenith angle = 53°, view zenith angle = 53°					
CH_4 and N_2O included in OSU calculations					
McClatchey atmosphere	Surface reflectance	Downward transmittance NASA	Downward transmittance OSU	TOA reflectance NASA	TOA reflectance OSU
MLS	0.2	0.788	0.748	0.137	0.124
MLS	0.7	0.788	0.748	0.478	0.436
Tropical	0.2	0.735	0.703	0.123	0.113
Tropical	0.7	0.735	0.703	0.431	0.395
CH_4 included, no N_2O in OSU calculations					
MLS	0.2	-	0.763	-	0.125
MLS	0.7	-	0.763	-	0.451
Tropical	0.2	-	0.717	-	0.117
Tropical	0.7	-	0.717	-	0.410
No CH_4, no N_2O in OSU calculations					
MLS	0.2	-	0.797	-	0.139
MLS	0.7	-	0.797	-	0.486
Tropical	0.2	-	0.748	-	0.126
Tropical	0.7	-	0.748	-	0.440
Effect of water vapor, CH_4 and N_2O included in OSU calculations					
MLW	0.2		0.86		0.154
MLW	0.7		0.86		0.538

Table 1 Comparison of transmittance and top-of-atmosphere reflectance calculations

CH_4 and N_2O included in OSU calculations				
McClatchey profile	Surface albedo	Top of atmosphere emission $\theta = 0.0°$	$\theta = 53.1°$	$\theta = 72.5°$
MLS	0.0	0.410	0.395	0.366
MLS	0.2	0.345	0.334	0.313
MLS	0.7	0.183	0.183	0.182
Tropical	0.0	0.521	0.497	0.454
Tropical	0.2	0.441	0.423	0.392
Tropical	0.7	0.241	0.240	0.237
CH_4 included, no N_2O in OSU calculations				
MLS	0.0	0.415	0.403	0.378
MLS	0.2	0.348	0.339	0.323
MLS	0.7	0.181	0.181	0.183
Tropical	0.0	0.527	0.507	0.470
Tropical	0.2	0.445	0.431	0.404
Tropical	0.7	0.239	0.239	0.239
No CH_4, no N_2O in OSU calculations				
MLS	0.0	0.421	0.412	0.394
MLS	0.2	0.352	0.346	0.334
MLS	0.7	0.179	0.181	0.186
Tropical	0.0	0.535	0.519	0.490
Tropical	0.2	0.451	0.439	0.419
Tropical	0.7	0.239	0.239	0.244

Table 2 Top-of-atmosphere emission calculations comparison

To gain further insight into possible sources of the discrepancies, pixel-level comparisons were performed for four scenes for which Langley provided VINT results. All of the comparisons were for single-layered, low-level, water clouds. VINT and OSU 0.63-μm optical depths, which depend primarily on sunlight reflected at 0.63-μm and are relatively insensitive to the retrieved cloud emission temperature and droplet radius, agree within acceptable bounds. VINT appears to branch to multiple solutions, some with optical depths that depart substantially from the OSU values. The branching may be caused by a mixed phase identification in VINT.

VINT and OSU cloud emission temperatures are generally within 1 K.

VINT and OSU effective droplet radii depart substantially, and the departures have characteristic dependencies on viewing geometry and droplet radii, suggesting that differences in the Mie and multiple scattering calculations, or the representation of the radiative transfer results in the retrieval schemes is the root of the differences.

When comparisons are restricted to a limited range of viewing geometries, e.g. nadir or limb, marked differences appear in the relationships used to extract droplet radius from 3.7-μm reflectances. VINT (observations-dots) returns much larger droplet radii for a given 3.7-μm reflectance than is given by the relationship used in the OSU retrievals (line-crosses). Some of the differences could be caused by differences in the contribution by emission calculated for the 3.7-μm radiances. Differences in estimates of the 3.7-μm reflected sunlight appear to grow as the 0.63-μm optical depth decreases. These trends are observed for both nadir and limb (direction of backscattered sunlight) views. Emission by opaque clouds is relatively insensitive to droplet radii. Nevertheless, even though there is almost no difference in the 3.7-μm

reflectance estimated for opaque clouds, differences in retrieved droplet radii remain. Evidently, there are substantial differences between the droplet radius to 3.7-μm reflectance relationships employed by VINT and OSU.

The comparison of pixel-scale VINT and OSU retrieved cloud properties contradicts the earlier finding by D. Young, NASA Langley, which indicated that the 3.7-μm reflectances calculated with and without atmospheric corrections by Langley and OSU were in agreement. Perhaps the VINT retrievals should be compared with the radiative transfer calculations used to produce them to determine whether the interpolation and parameterization schemes used in the retrievals are retaining the correct relationships. The retrieved products for the OSU scheme are consistent with the results of the radiative transfer calculations.

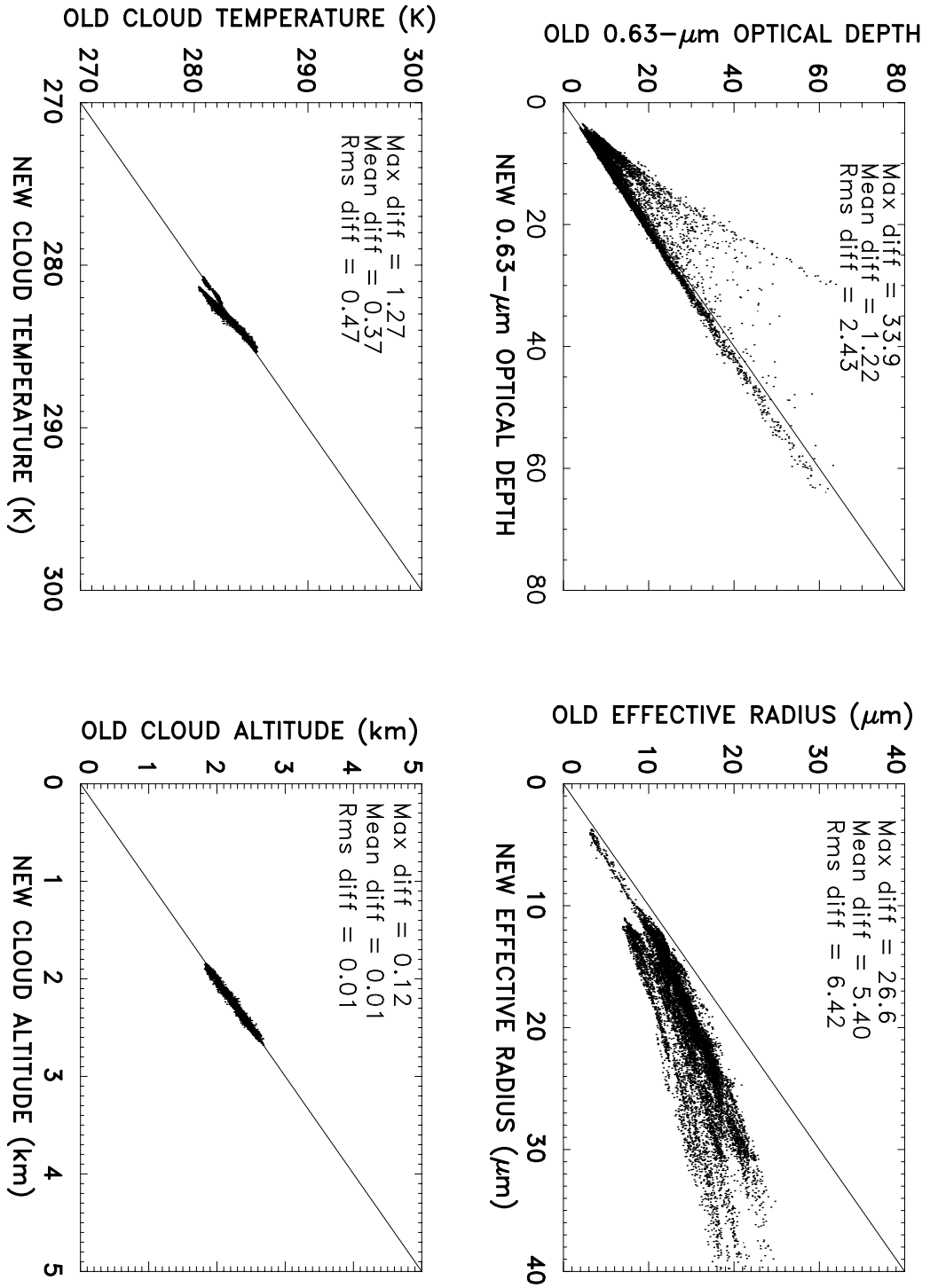

Comparison between previous retrieval results and the new, corrected version demonstrate the improvement of optical depth retrievals from correcting the azimuth angle, and the larger effective radii obtained with the corrected filter response function.

Change in 3.7-μm Reflected Radiance due to Change in Filter Function

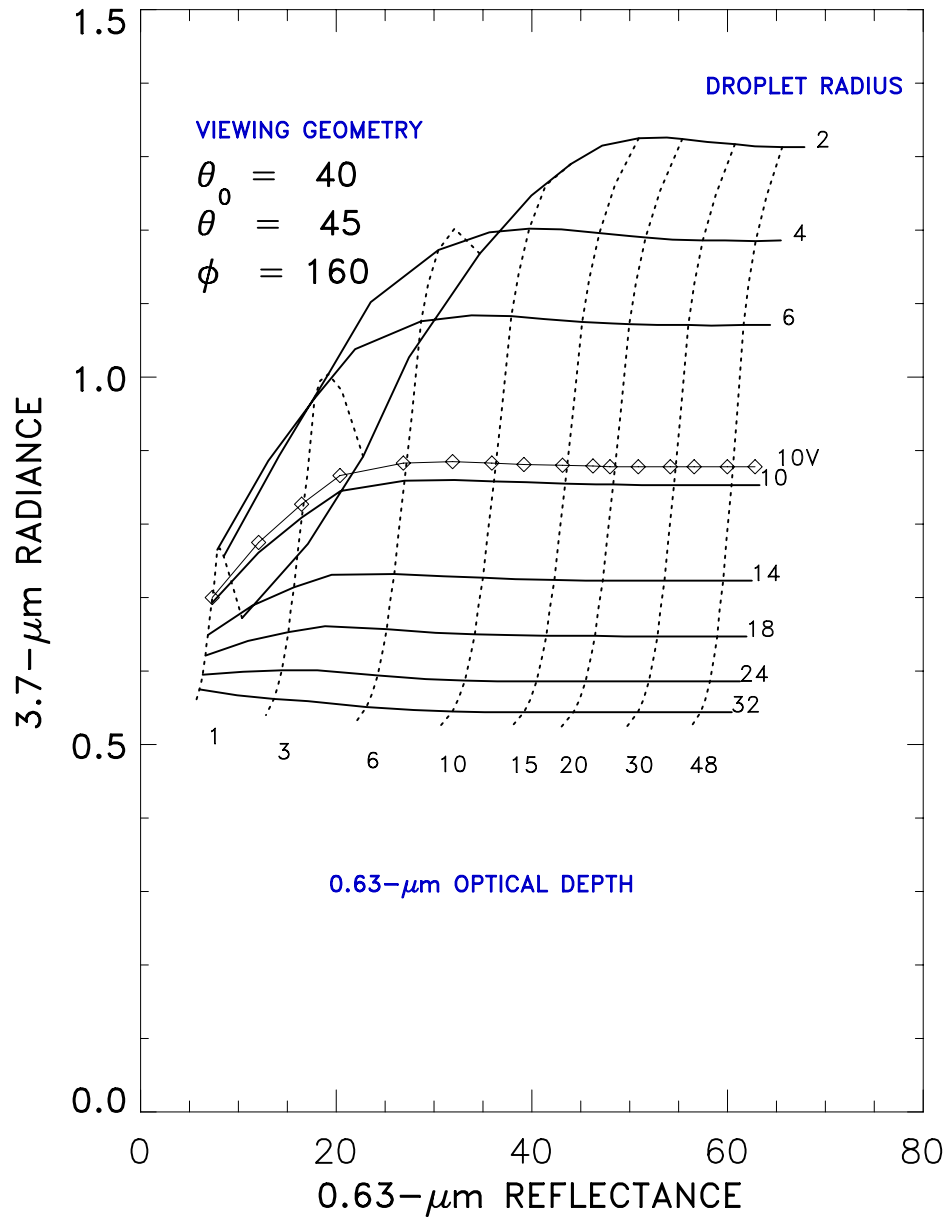

0.63-μm reflectance and 3.7-μm radiance calculated for the indicated viewing geometry. The line identified as 10V is for reflected sunlight obtained with the corrected filter function. The sunlight is reflected by a cloud with 10-μm droplets.

VINT and OSU Optical Depths

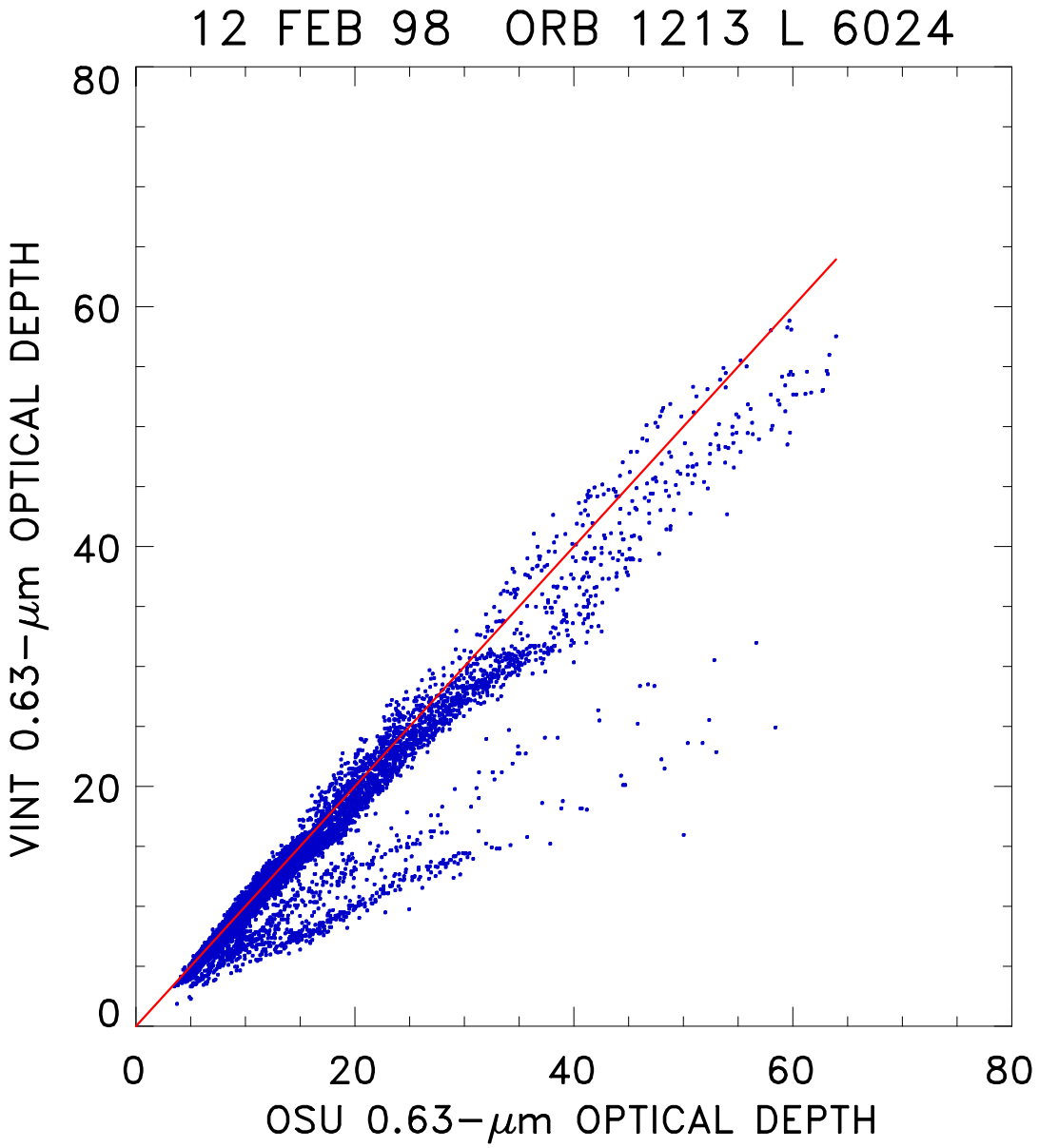

VINT and OSU optical depths for pixels overcast by low-level, single-layered, water clouds. The line indicates perfect agreement.

VINT and OSU Cloud Emission Temperature

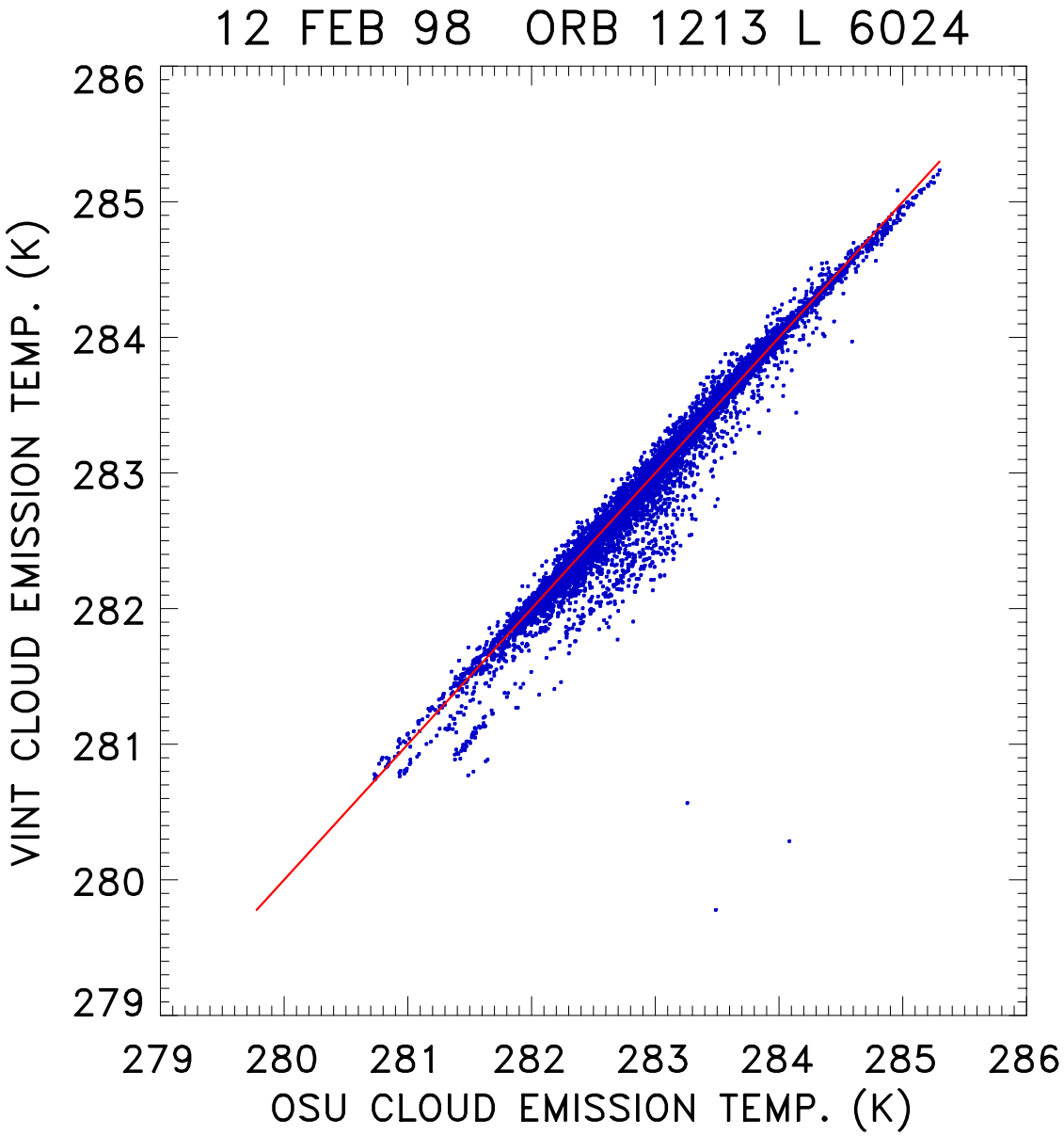

VINT and OSU cloud emission temperatures (K) for pixels overcast by single-layered, low-level water clouds. Line indicates perfect agreement.

VINT and OSU Droplet Effective Radius

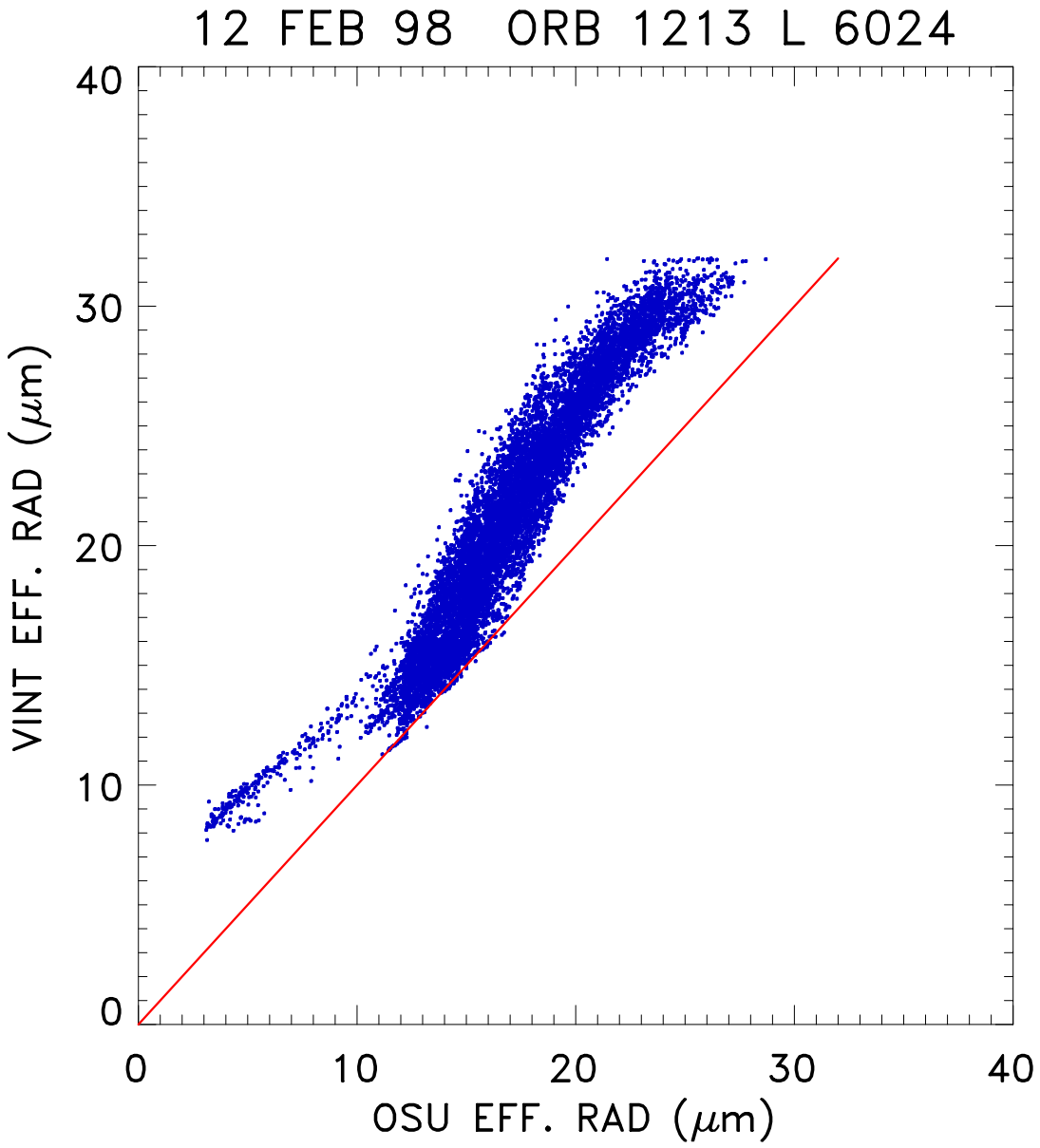

VINT and OSU droplet effective radius for pixels overcast by single-layered, low-level, water clouds. Line indicates perfect agreement.

Difference in Effective Radius and Satellite Zenith Angle

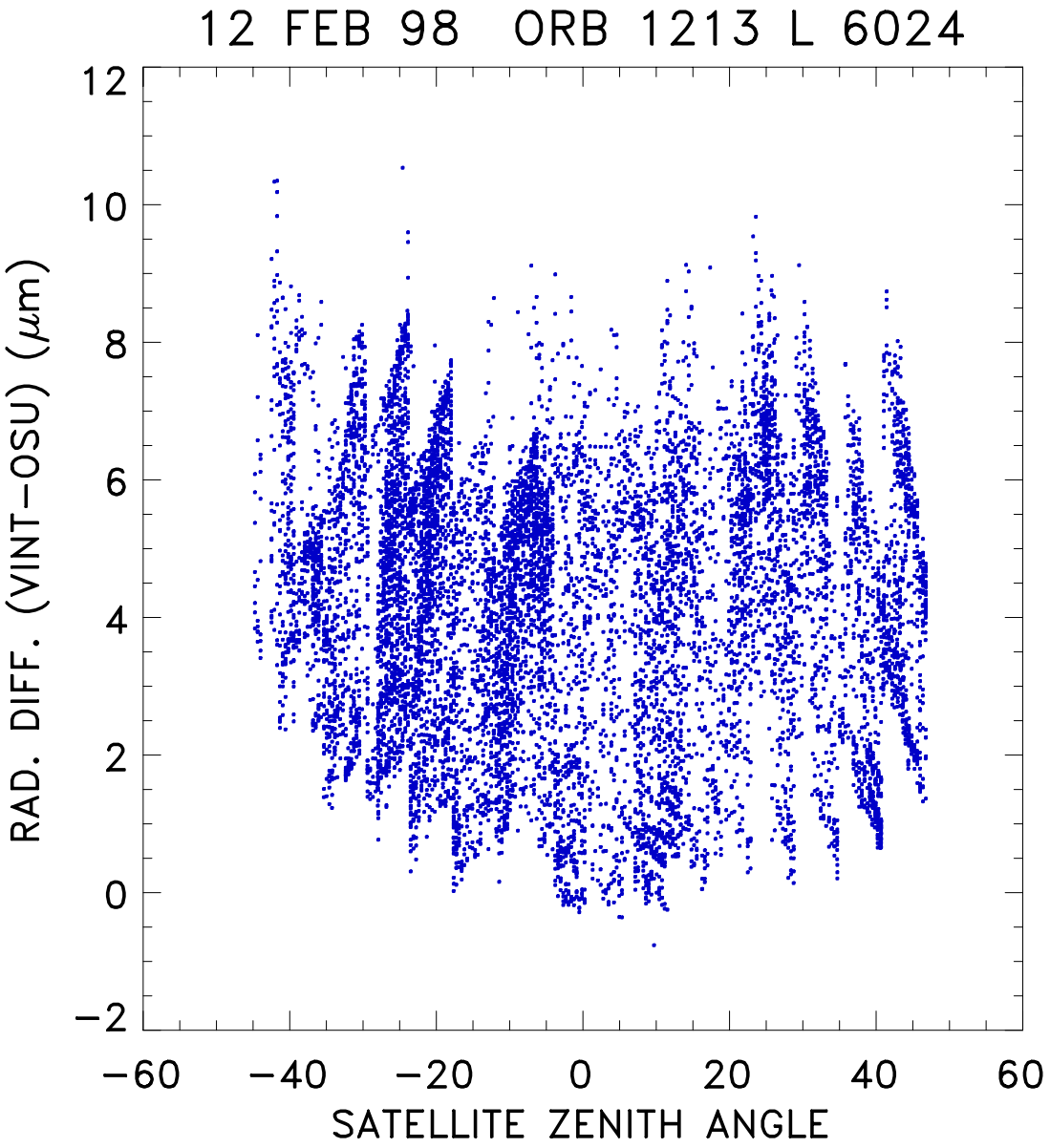

Difference in retrieved droplet effective radius and satellite zenith angle. Negative satellite zenith angles indicate direction of backscattered sunlight.

VINT and OSU 3.7-μm Reflectance and Droplet Effective Radius

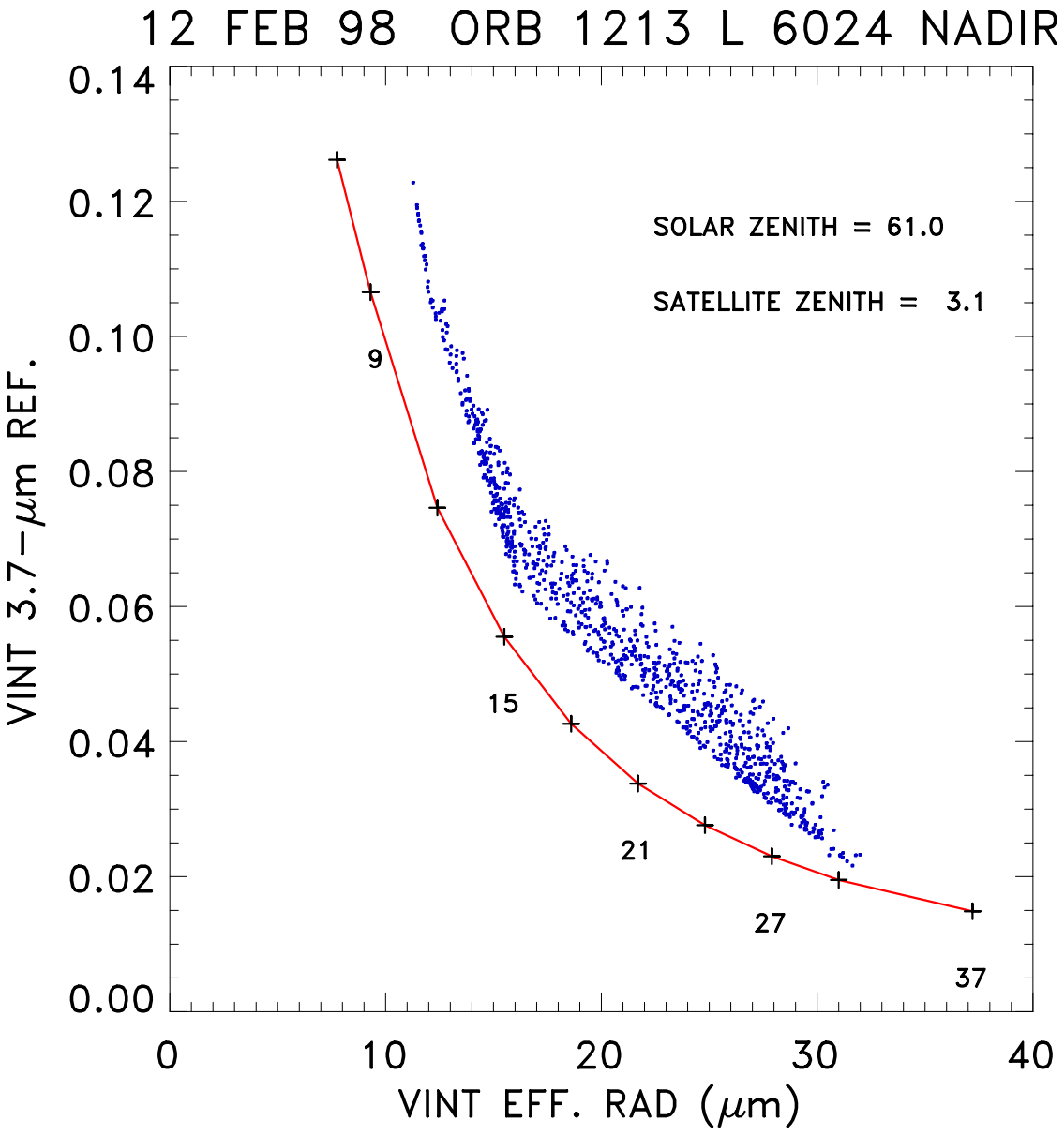

VINT (dots) and OSU (line and crosses) 3.7-μm reflectance and droplet effective radius. The observations are of 3.7-μm reflectances at satellite zenith angles less than 5° as obtained from VINT. Numbers below the crosses indicate the effective radius associated with the reflectance as obtained by the OSU retrieval scheme.

Difference in 3.7-μm Reflectance and 0.63-μm Optical Depth

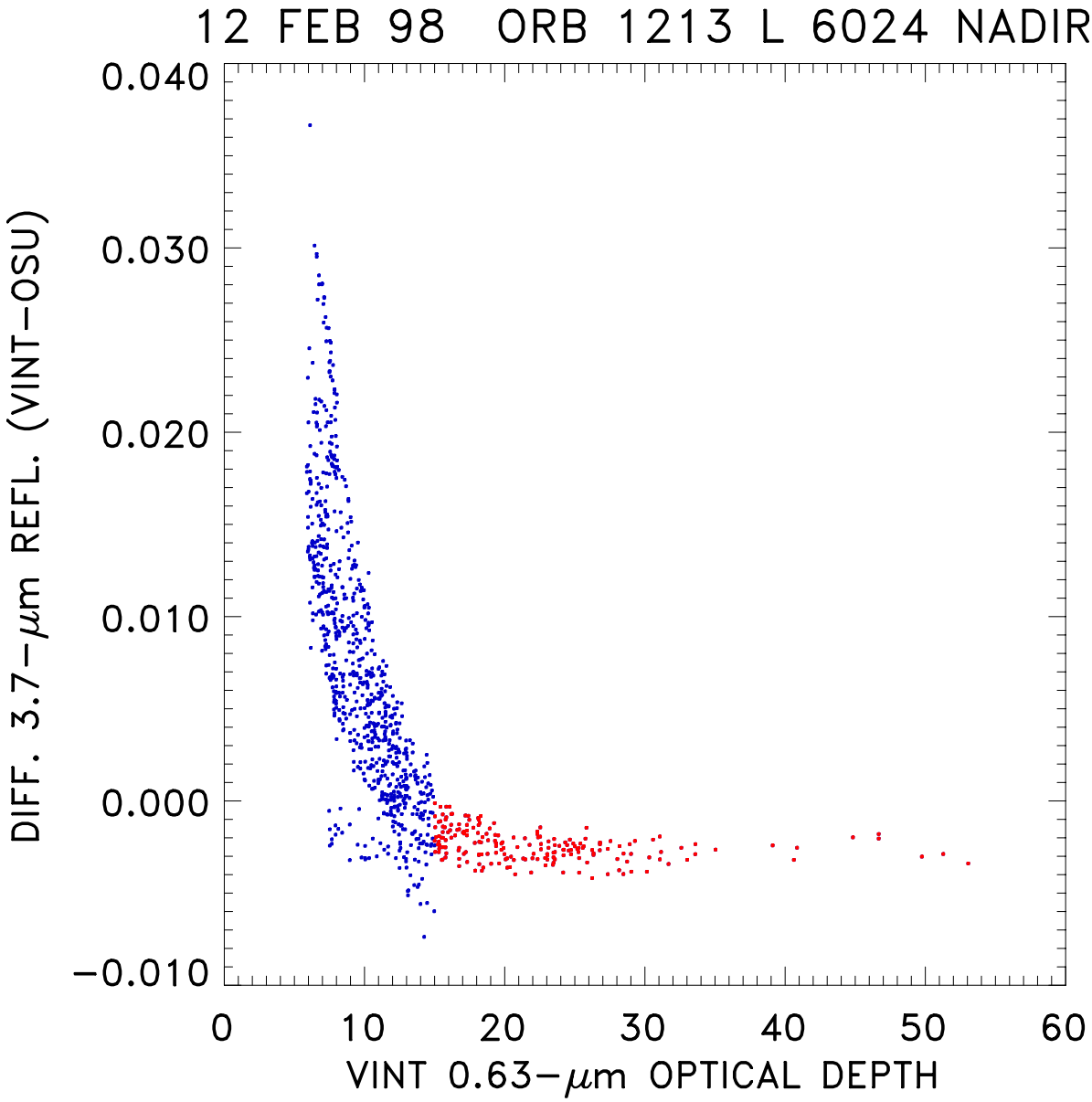

Differences in VINT and OSU-derived 3.7-μm reflectances and the VINT-derived 0.63-μm optical depth. Red dots identify clouds that are taken to be opaque at 3.7 μm. Observations are for satellite zenith angles less than 5°.

VINT and OSU 3.7-μm Reflectance and Droplet Effective Radius

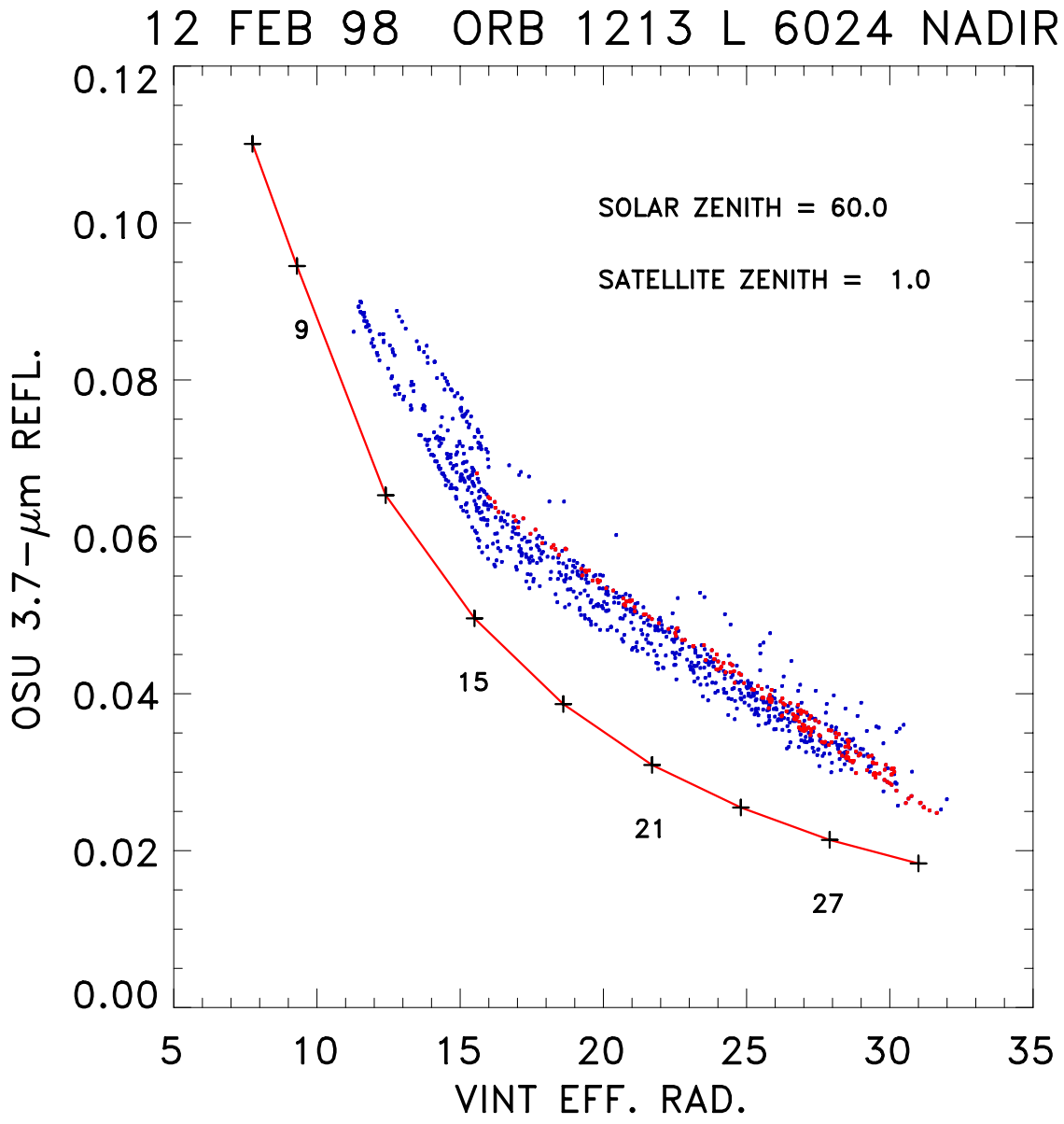

OSU (line, crosses, and dots) 3.7-μm reflectance and droplet effective radius and VINT droplet effective radius. The observations are of 3.7-μm reflectances at satellite zenith angles less than 5° as obtained from the OSU retrieval. Numbers below the crosses indicate the effective radius associated with the reflectance for the OSU retrieval. Red dots identify opaque clouds.

OSU 3.7-μm Reflectance and Droplet Effective Radius

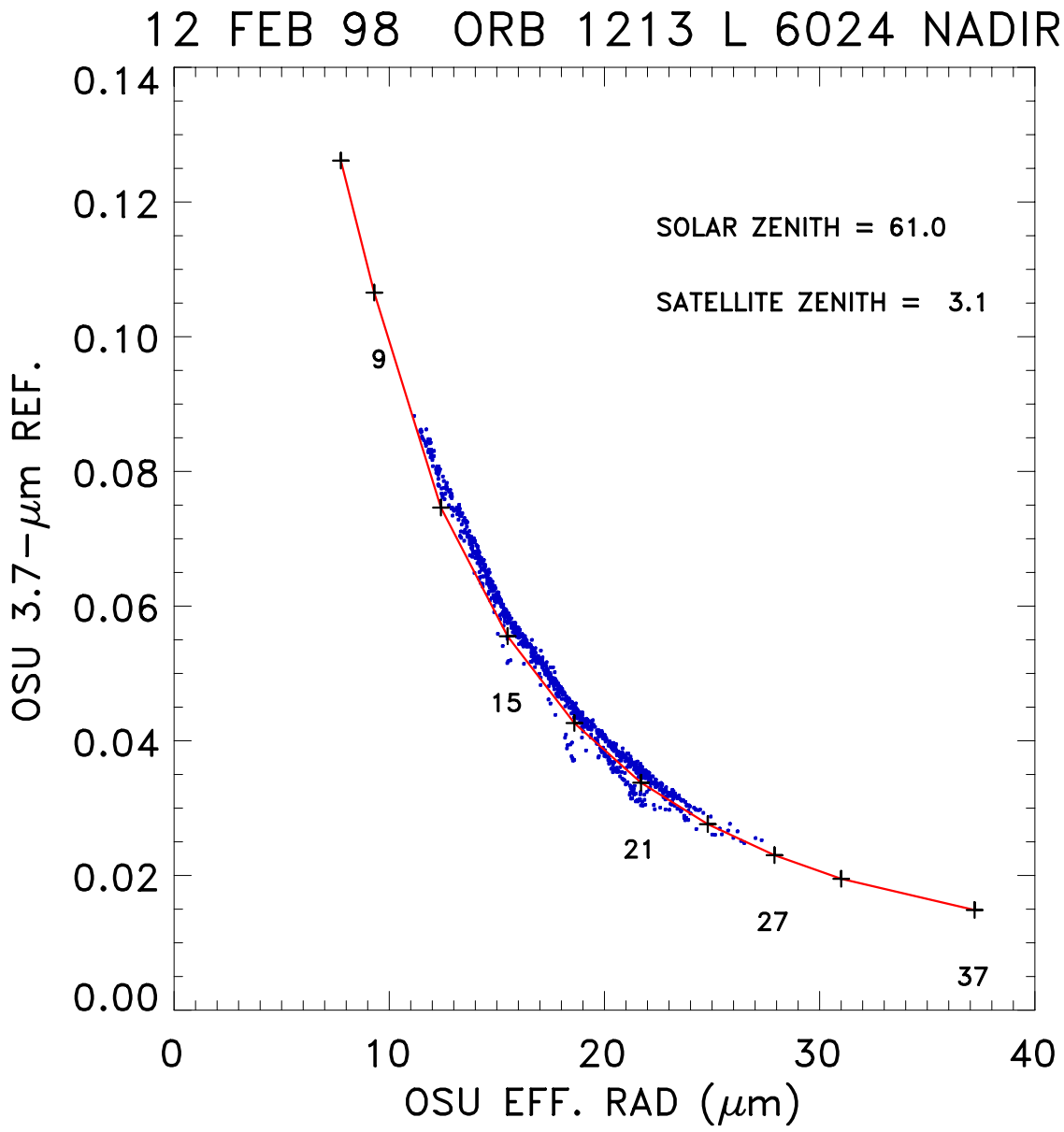

OSU 3.7-μm reflectance and droplet effective radius. The observations are of 3.7-μm reflectances at satellite zenith angles less than 5° obtained by the OSU retrieval scheme. The line and crosses represent results from plane-parallel radiative transfer calculations. Deviations from theory are due to variations of viewing geometry and cloud top altitudes within the scene.

VINT and OSU 3.7-μm Reflectance and Droplet Effective Radius

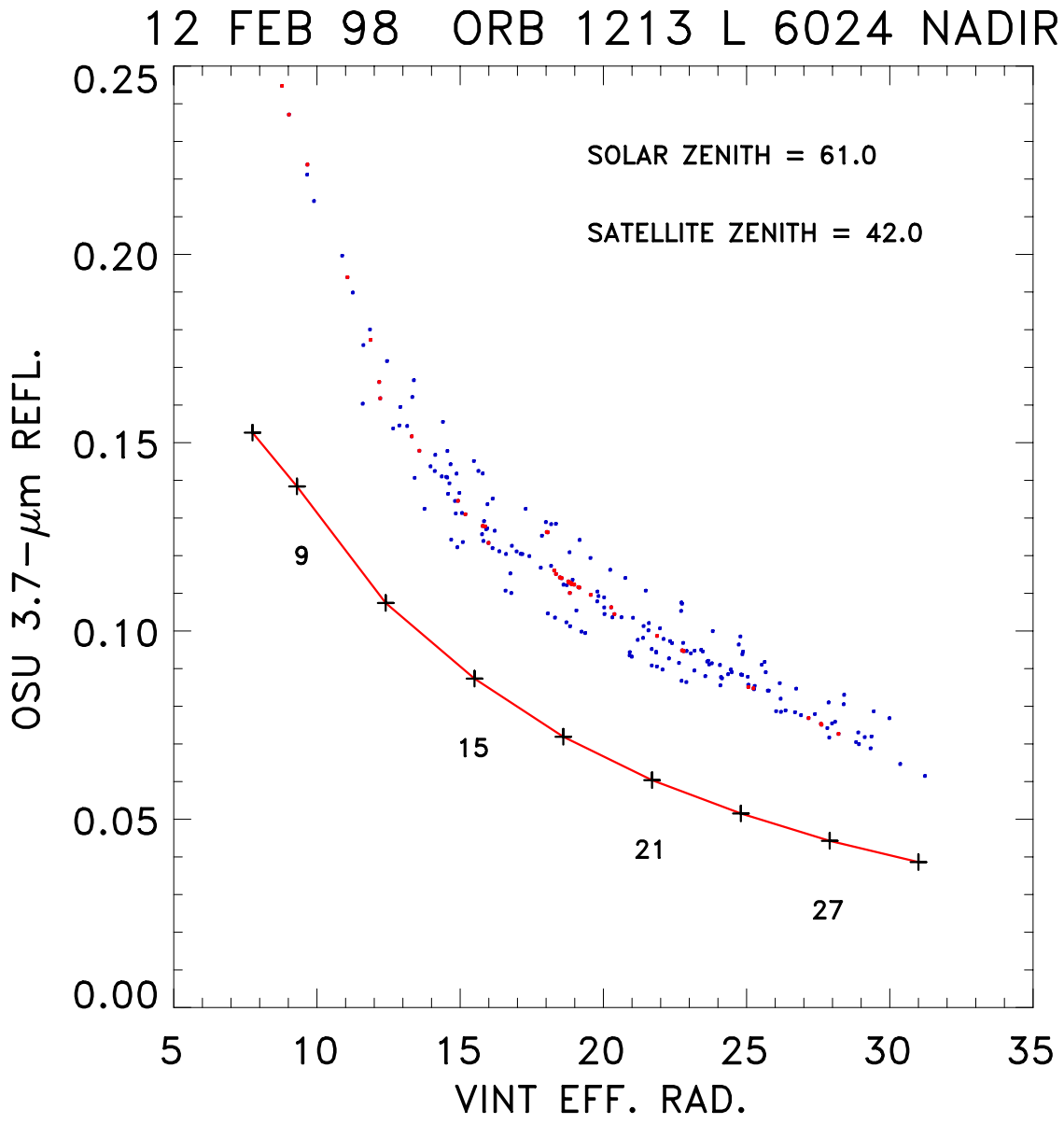

OSU (line, crosses, and dots) 3.7-μm reflectance and droplet effective radius and VINT droplet effective radius. The observations are of 3.7-μm reflectances at satellite zenith angles greater than 40° in the direction of backscattered sunlight as obtained from the OSU retrieval. Red dots indicate opaque clouds.

OSU 3.7-μm Reflectance and Droplet Effective Radius

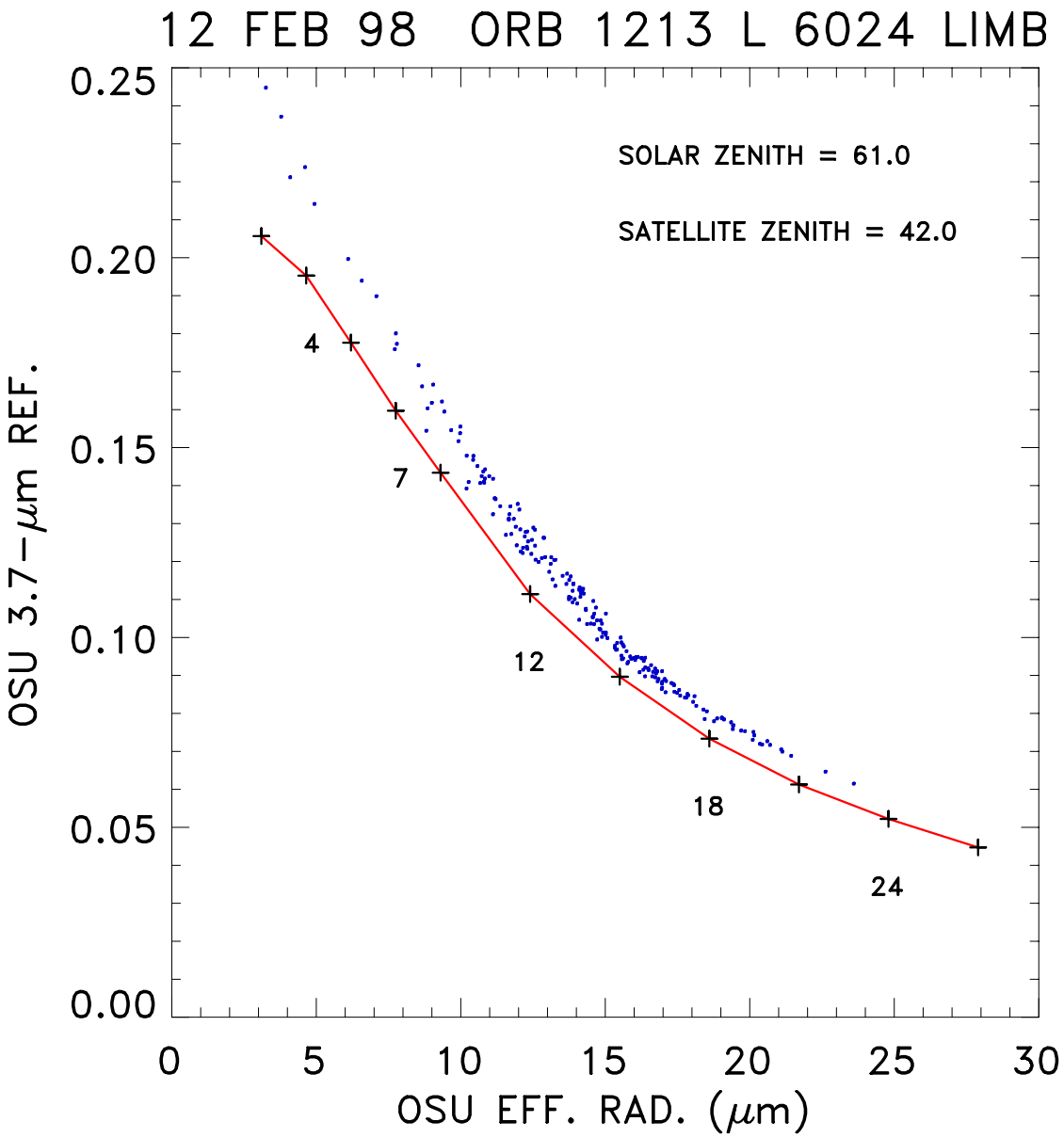

OSU 3.7-μm reflectance and droplet effective radius. The observations are of 3.7-μm reflectances at satellite zenith angles greater than 40° as obtained by the OSU retrieval scheme.

Evaluation and Comparison of Overcast and Partly Cloudy Retrievals

The algorithm for retrieving the droplet radius, 0.63-μm optical depth, and fractional cloud cover for partly cloudy pixels has been updated and is being evaluated. Partly cloudy pixels are assumed to have the same cloud altitude and temperature as nearby overcast pixels, and to have observed radiances given by

$$I = I_s(1 - A_c) + A_c I_c$$

where I_s is the radiance associated with the cloud-free portions of the region and is derived from the cloud-free pixels; A_c is the fractional cloud cover and is derived as part of the retrieval; and I_c is the radiance associated with the overcast portions of the pixel and is also derived as part of the retrieval.

The clouds for the partly cloudy pixels are presumed to have the same emission temperatures as the clouds for the pixels identified as being overcast. The initial 0.63-μm optical depth and droplet radius for the partly cloudy pixels are assumed to be the same as for the overcast pixels. Cloud fraction is retrieved from the observed 11-μm radiances and emission calculated for the cloud-free and overcast portions of the pixel. The 0.63-μm optical depths for the partly cloudy pixels are then varied to match the reflectances observed for these pixels. This derived optical depth is used to calculate the reflected, transmitted, and emitted components of I_c. An iterated value for A_c is then calculated until A_c converges to within 0.05.

The 3.7-μm emission for the overcast and cloud-free portions of the field of view are calculated and subtracted from the observed radiance to obtain the reflected component for the overcast portion. The droplet radius is then adjusted to achieve agreement between observed and calculated reflected radiances. These steps are iterated until the change in droplet radius is less than 1 μm.

Surface reflectance has been assumed to be zero for 0.63 and 3.7 μm. Comparisons of 3.7-μm radiances for cloud-free daytime and nighttime ocean scenes show that there are no differences between daytime and nighttime values. The observations agree closely with the calculated emission for near nadir satellite zenith angles.

To aid in evaluating the accuracy of the overcast retrievals, a regenerated radiance comparison was performed. The retrieved properties were used to generate radiances, and the regenerated radiances were used to retrieve a secondary set of cloud properties. This analysis was performed on individual samples, as well as on the whole optical depth and particle radius domain for all angular geometries. Individual samples of overcast VIRS pixels gave regenerated radiances within 2% of the original radiances for the 3.7-μm channel, and less than 1% for the 0.63-μm and 11-μm channels. The re-derived cloud properties were within the convergence criteria of 1 unit for optical depth, 1 μm for particle radius, and 1 K for cloud emission temperature. Retrievals that did not converge within the criteria for the whole domain were limited to regions of multiple solutions and extreme values for particle radius and optical depth. Regenerated radiances and re-derived cloud properties also agreed closely with original values for individual examples of partly cloudy retrievals.

The pixel-level radiances and overcast and partly cloudy retrieval products for a subregion in one of the 20 NASA-Langley/OSU comparison scenes discussed in the previous report (980210, 21:27) has been examined closely. Calculated and observed 0.63-μm reflectances and 11-μm radiances were compared. The overcast pixels (red) directly overlay the calculated values, demonstrating that the infrared emission is in good agreement. Partly cloudy pixels are green and cloud-free pixels are blue. Calculated and observed 0.63-μm reflectances and 3.7-μm radiances show that the overcast pixels have effective radii mostly in the range of 16 to 24 μm. The presence of partly cloudy pixels outside the calculated overcast domain may be due to cloud temperature and altitude variations, three dimensional effects, particle size variation within the cloud, surface reflectance, or inaccurate retrievals. Further investigation is underway.

The cloud fraction distribution for this subregion shows that most of the partly cloudy pixels have cloud fractions of 0.75 to 0.90. The retrieved properties for the partly cloudy pixels in the subregion were

examined for relationships between cloud fraction, effective radius, and optical depth. Effective radius shows a dependence on cloud fraction, especially in the range of 4 to 15 μm. Optical depth also shows a dependence on cloud fraction, with higher optical depth values at larger cloud fractions. The higher optical depth and effective radius values at the lowest cloud fractions suggest the possible presence of some surface reflection. This issue will be explored further.

Optical depth and effective radius retrievals for the partly cloudy pixels were compared to those of the overcast retrievals. The mean optical depth for the partly cloudy pixels was about 8 units less than the mean overcast optical depth. The mean partly cloudy effective radius was about 9 μm smaller than the mean overcast value.

As a followup analysis, retrievals were performed for partly cloudy pixels with cloud fraction greater than 0.20, in which these pixels were retrieved as if they were overcast. Pixels with cloud fractions less than 0.20 were not included since very small cloud fractions can be considered more like clear-sky than overcast. The results give a new mean optical depth that was several units smaller than if the pixels were treated as partly cloudy. However, the new mean effective radius was about 3 μm larger than if these pixels were retrieved as partly cloudy.

The pixel-level radiances and retrieval products from a subregion of a separate VIRS scene (980222, 19:57) has also been analyzed. This subregion has a quite different cloud fraction distribution, with most of the partly cloudy pixels having cloud fractions below 0.30. A weak dependence of effective radius on cloud fraction was found, along with a wide range of effective radii for the smallest cloud fractions. The partly cloudy pixels with cloud fractions greater than 0.20 were retrieved as if they were overcast and compared to the partly cloudy retrieval results. The mean retrieved optical depth decreased by about 3, and the mean effective radius increased by just over 3 μm compared to those for the partly cloudy retrievals.

The overcast and partly cloudy retrieval analyses performed so far reveal a number of issues needing continued investigation. Future work includes refinement and more testing of the partly cloudy retrieval scheme, and further exploration of the overcast/partly cloudy retrieval results, including investigating sensitivities to cloud altitude. The effects on radiative fluxes will be examined. The addition of realistic surface reflectance models, methods for the separation of cloud layers for multilayered systems, and an investigation of the vertical distribution of cloud properties is also planned.

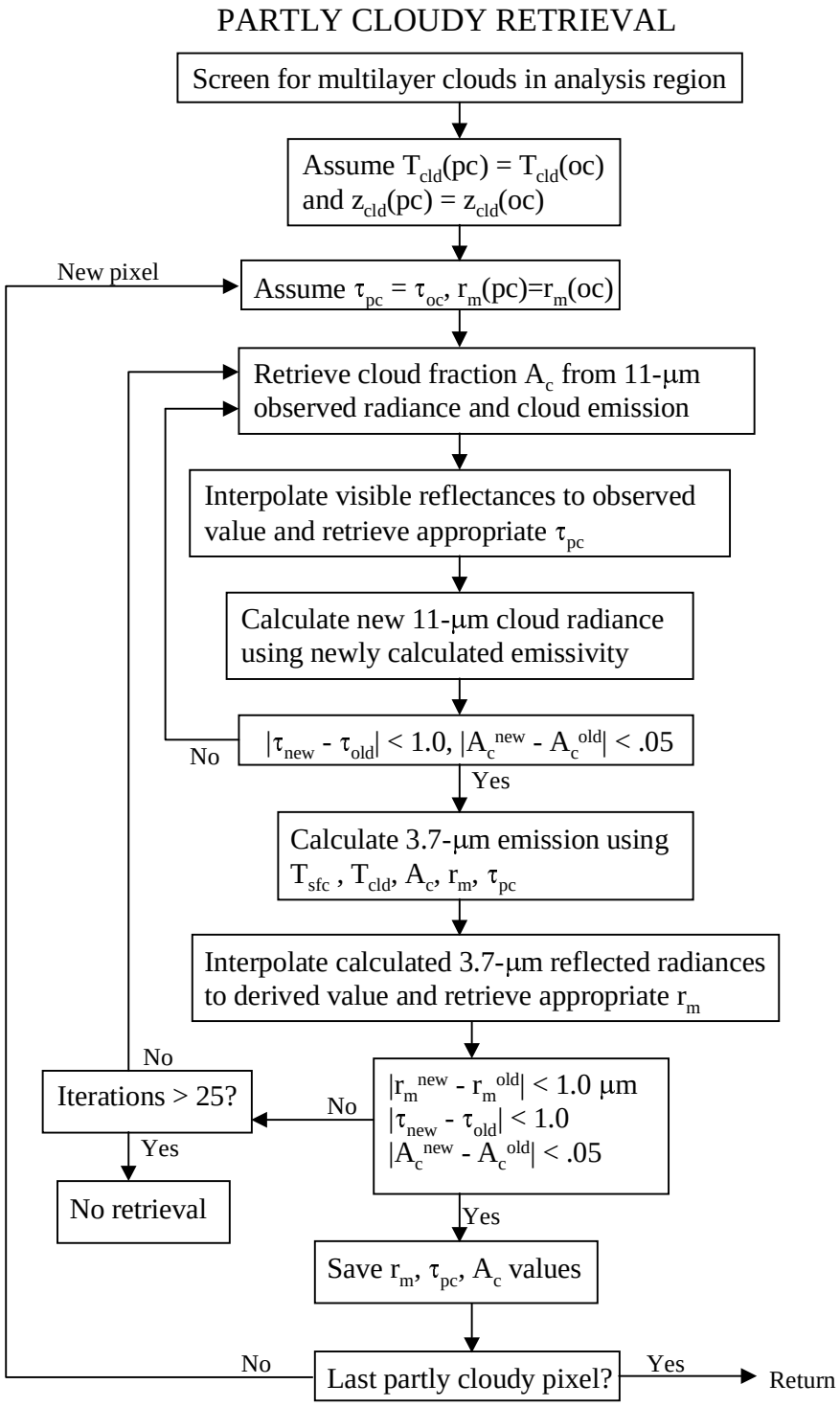

Partly cloudy retrieval algorithm contains a calculation of the emitted, transmitted, and reflected radiance at 11 μm for each iteration until convergence of cloud fraction to 0.05.

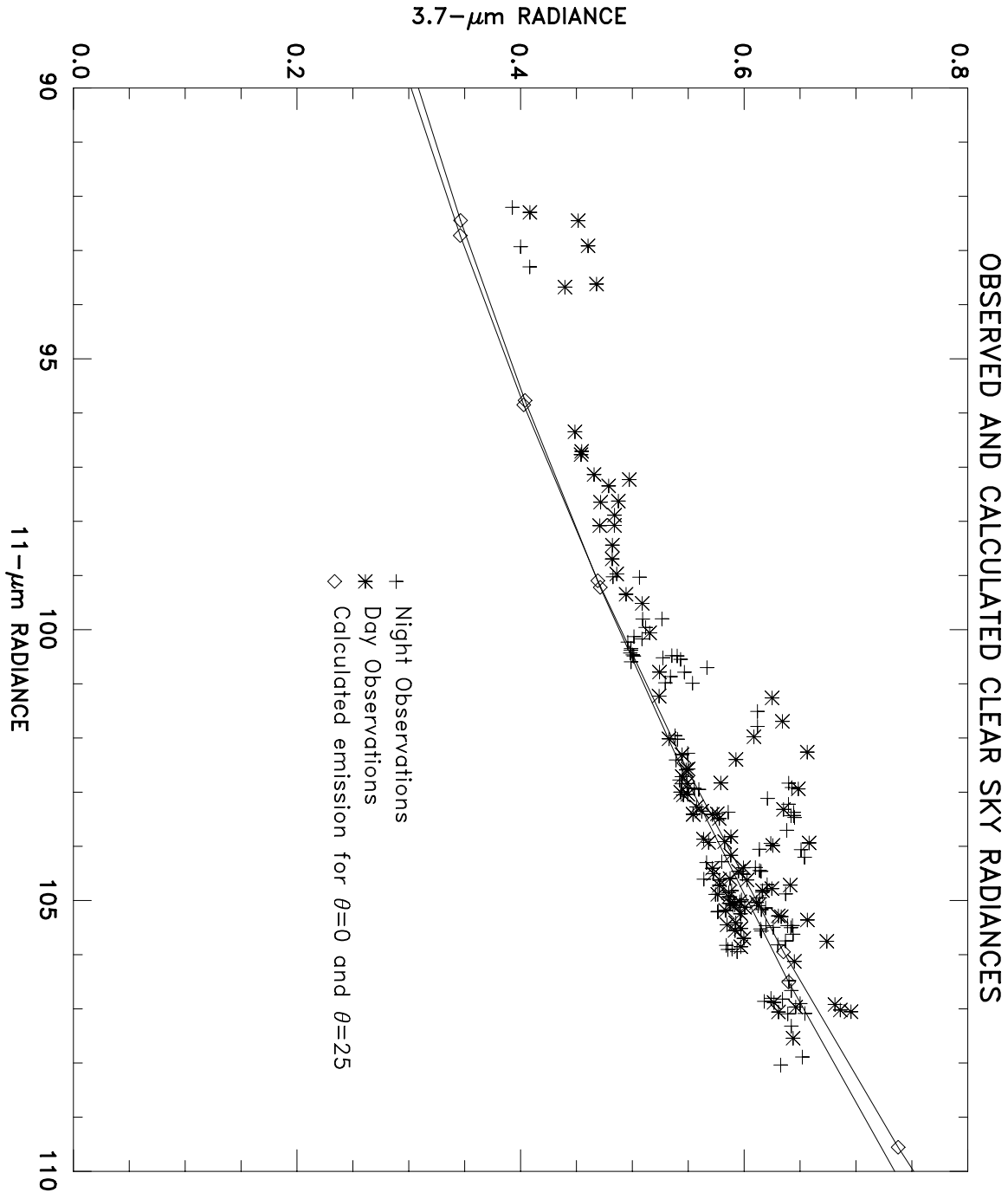

Daytime backscattered and nighttime clear sky radiance observations at 3.7 μm and 11 μm overlay each other and agree with calculated emission, showing that the reflected component is negligible.

PARTLY CLOUDY RETRIEVAL PRODUCTS

980210 21:27

TEMPERATURES

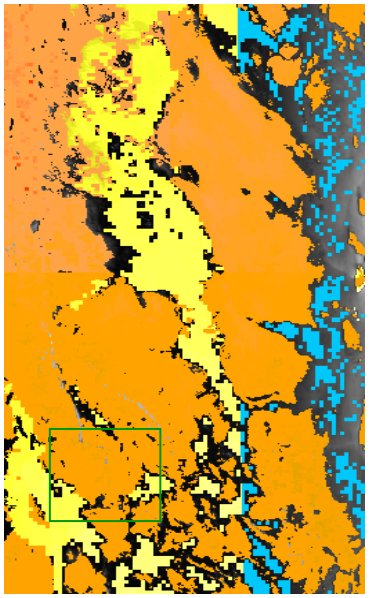

OPTICAL DEPTHS

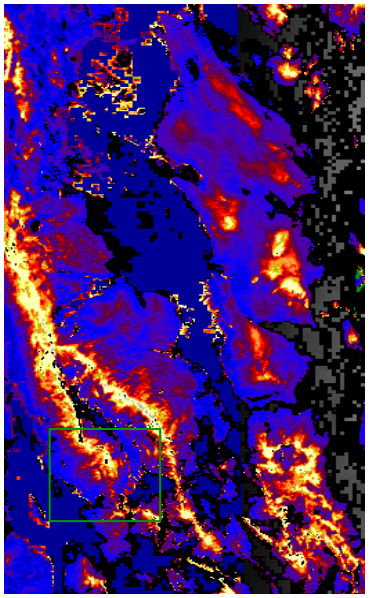

DROPLET RADII

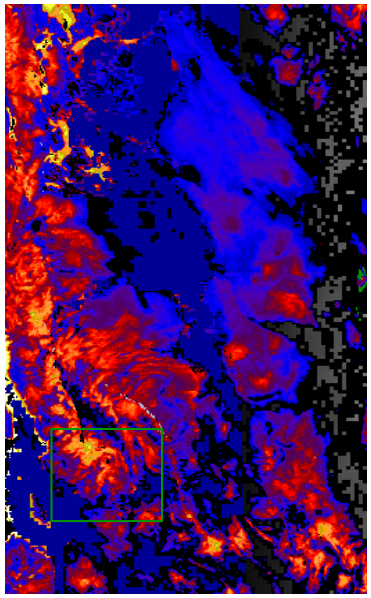

CLOUD FRACTION

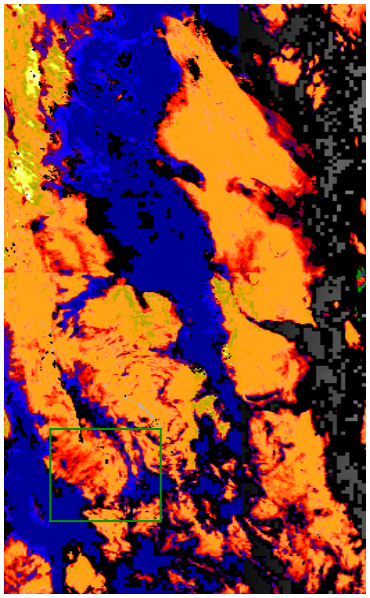

T=250 K	275 K	300 K
τ=1	32	64
r=2 μm	20 μm	40 μm
Ac=0%	100%	

Partly cloudy retrieval products from a subregion of one of the previously identified comparison scenes have been analyzed more closely.

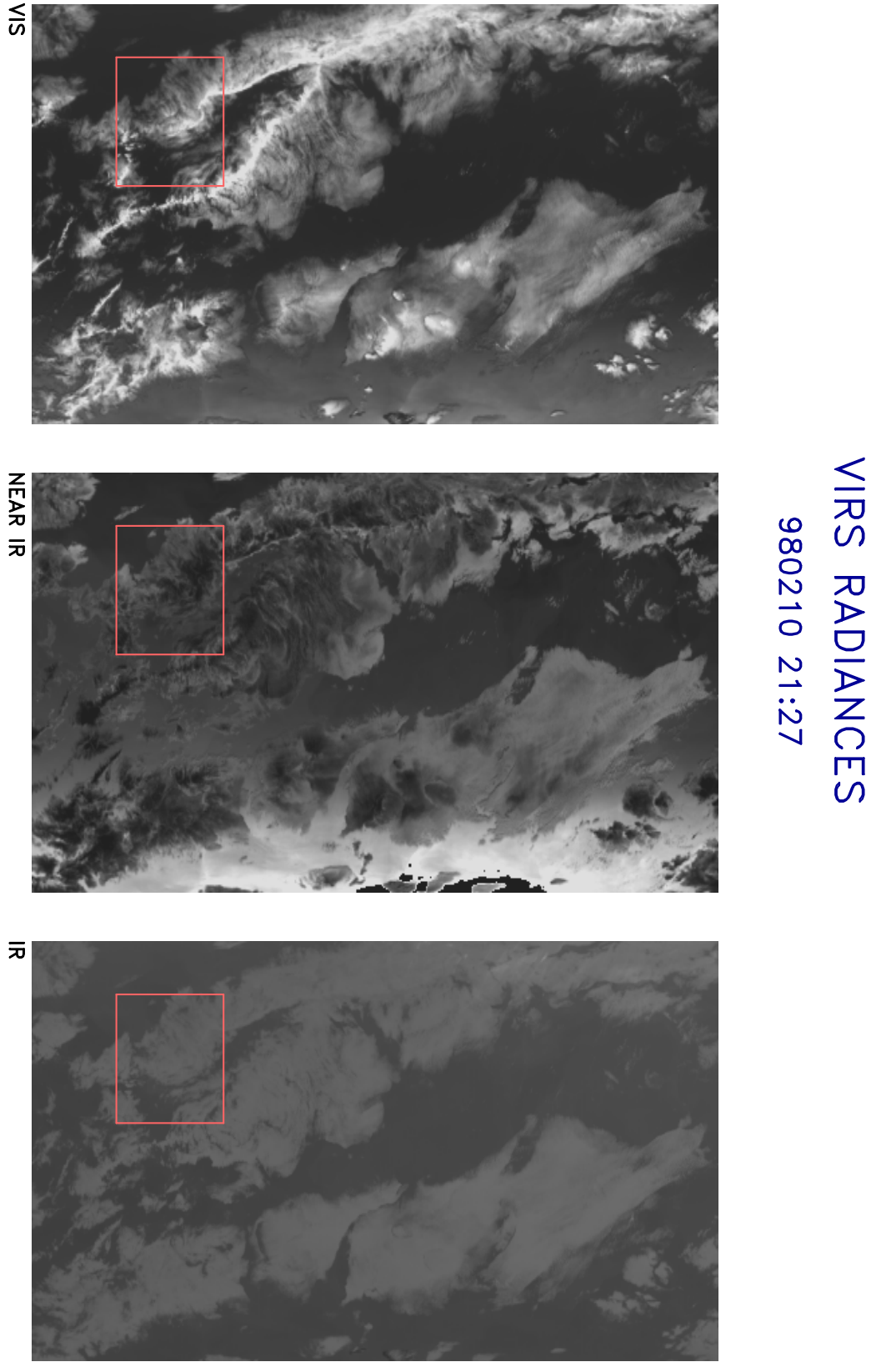

The corresponding pixel-level radiances for the comparison scene are shown, with the analysis region outlined.

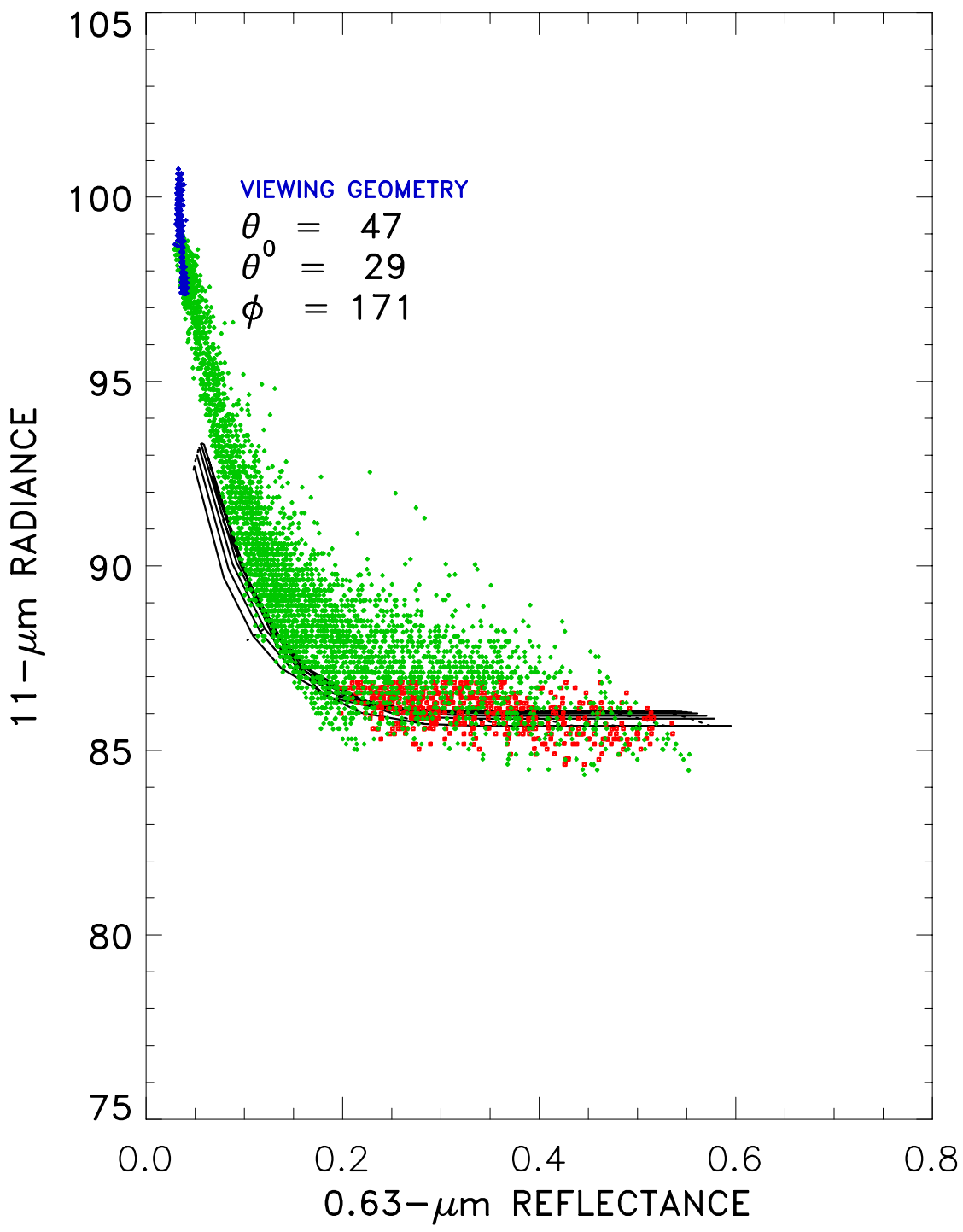

Observed 0.63 and 11-μm overcast radiances (red) directly overlay the calculated values, showing that the infrared emission is in good agreement with observations. Partly cloudy pixels are green, and cloud-free pixels are blue.

CALCULATED AND OBSERVED RADIANCES

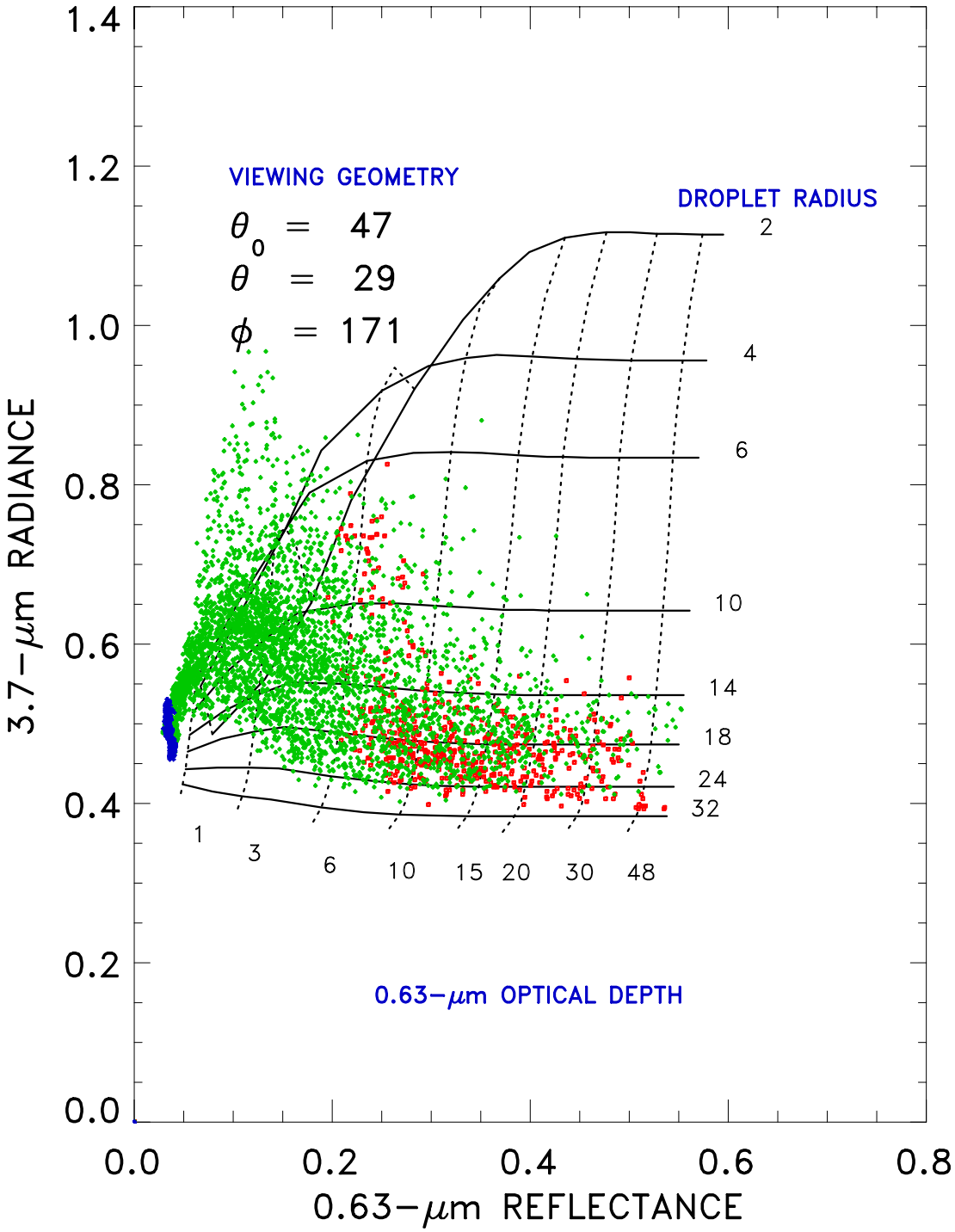

Calculated and observed 0.63 and 3.7-μm radiances show that overcast pixels (red) have effective radii between 16-24 μm. Partly cloudy pixels (green) outside the calculated overcast domain may be due to a number of different factors.

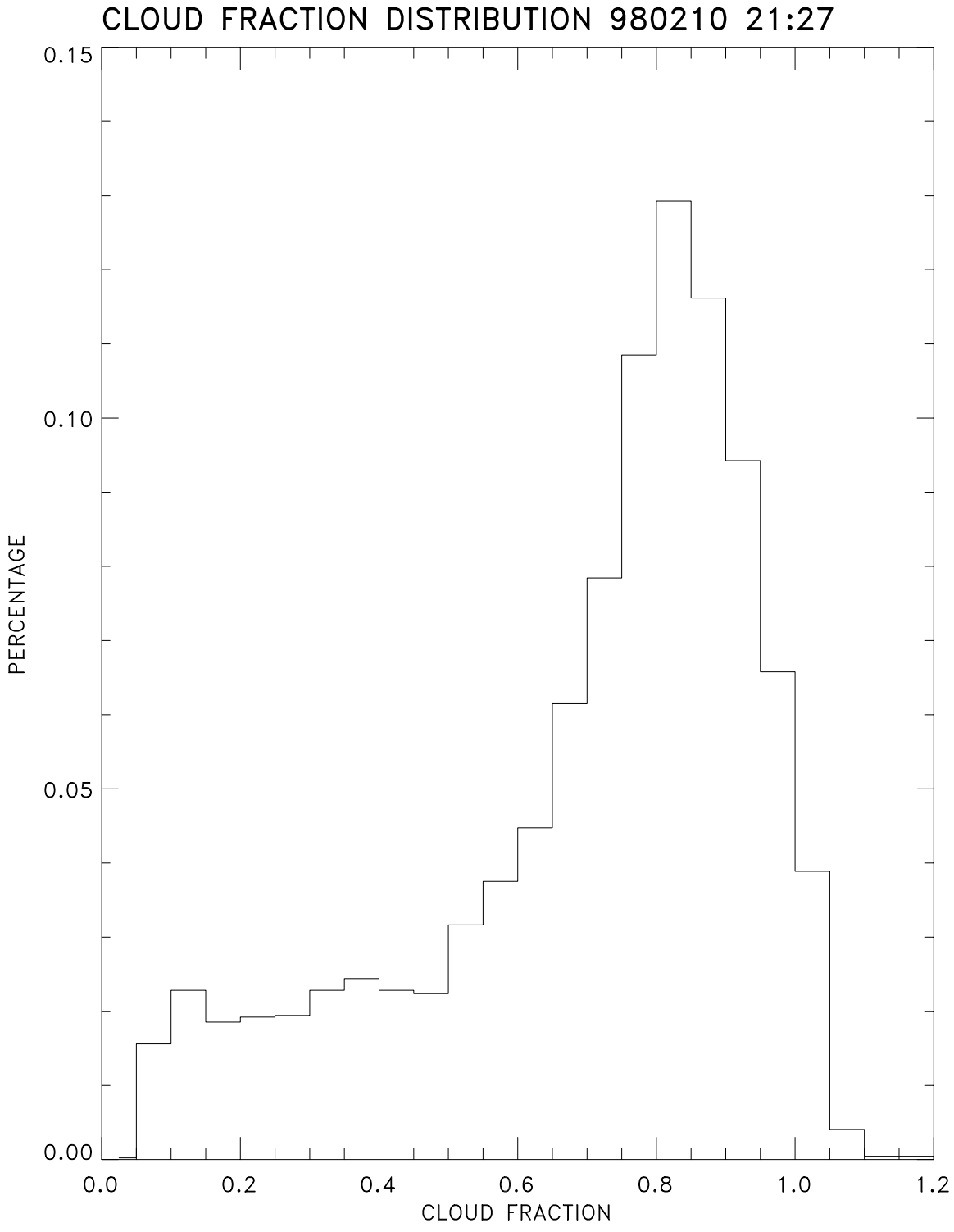

The cloud fraction distribution for this subregion is weighted toward higher cloud fractions, with most of the partly cloudy pixels having cloud fractions between 0.75 and 0.90.

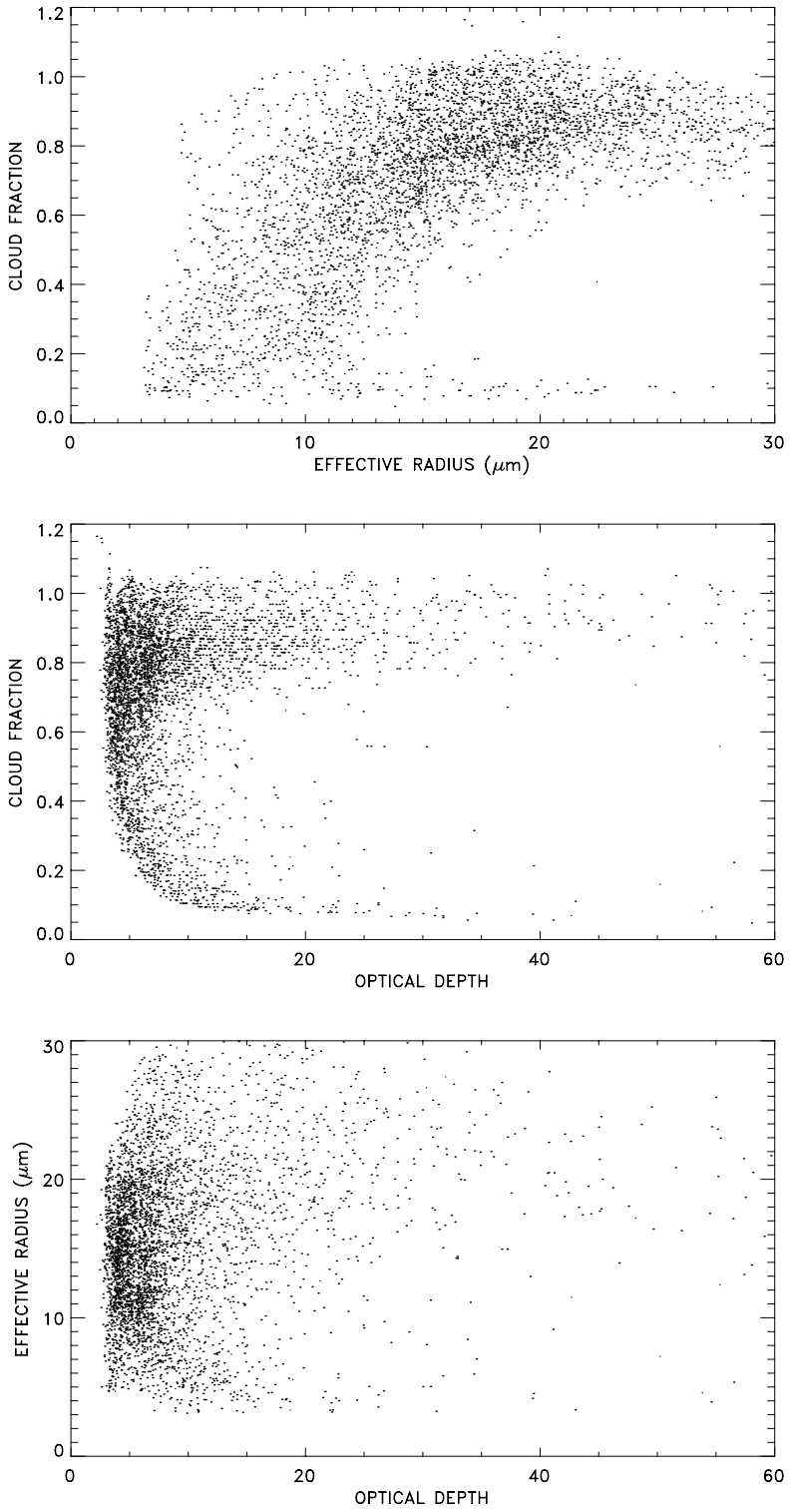

Retrieved effective radius shows a dependence on cloud fraction, especially between 4 and 15 μm. Optical depth also shows a dependence on cloud fraction, with higher optical depths at larger cloud fractions.

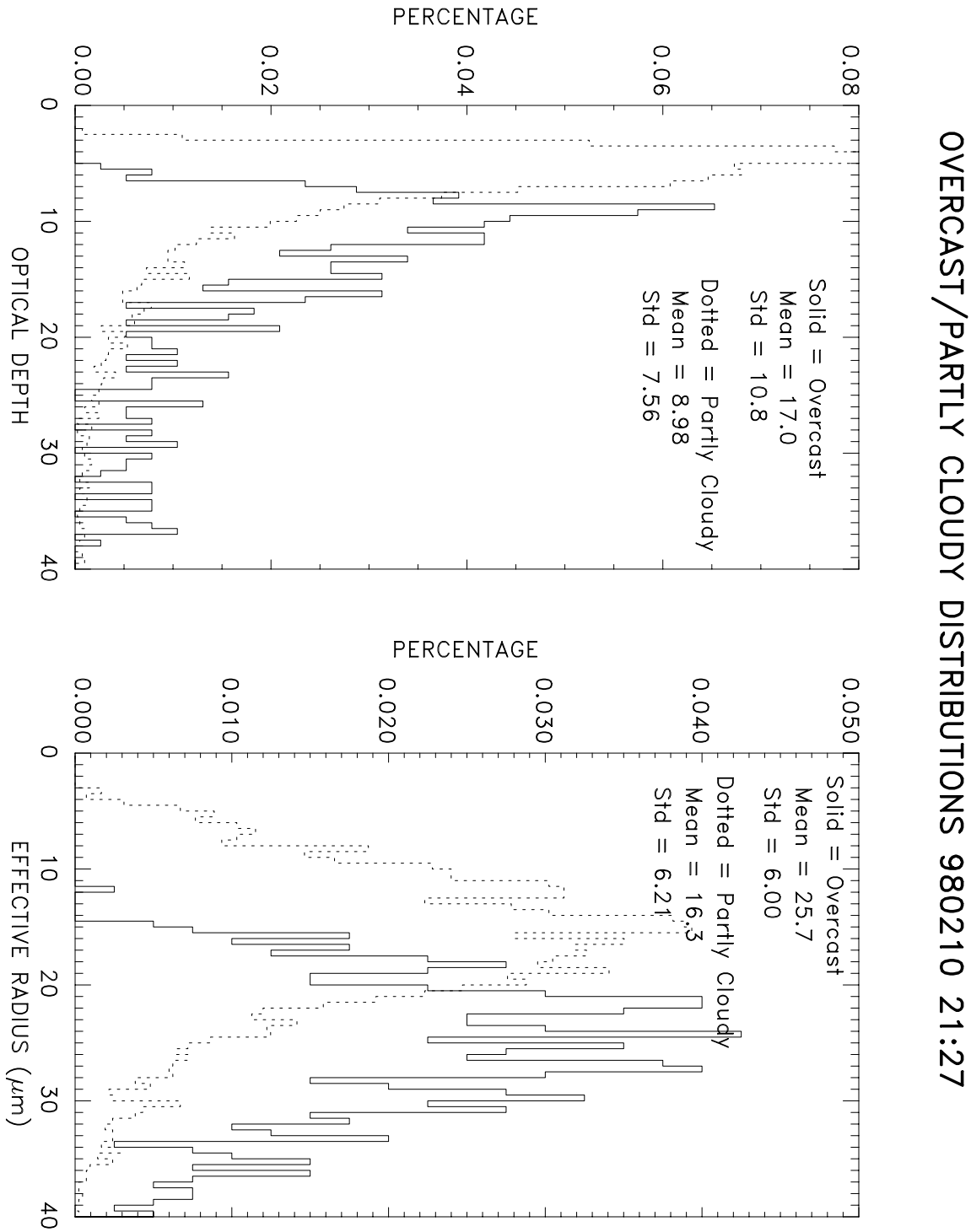

Distributions of overcast and partly cloudy optical depth and effective radius retrievals show marked differences for this subregion. Partly cloudy retrievals have optical depths and effective radii much smaller than the overcast values.

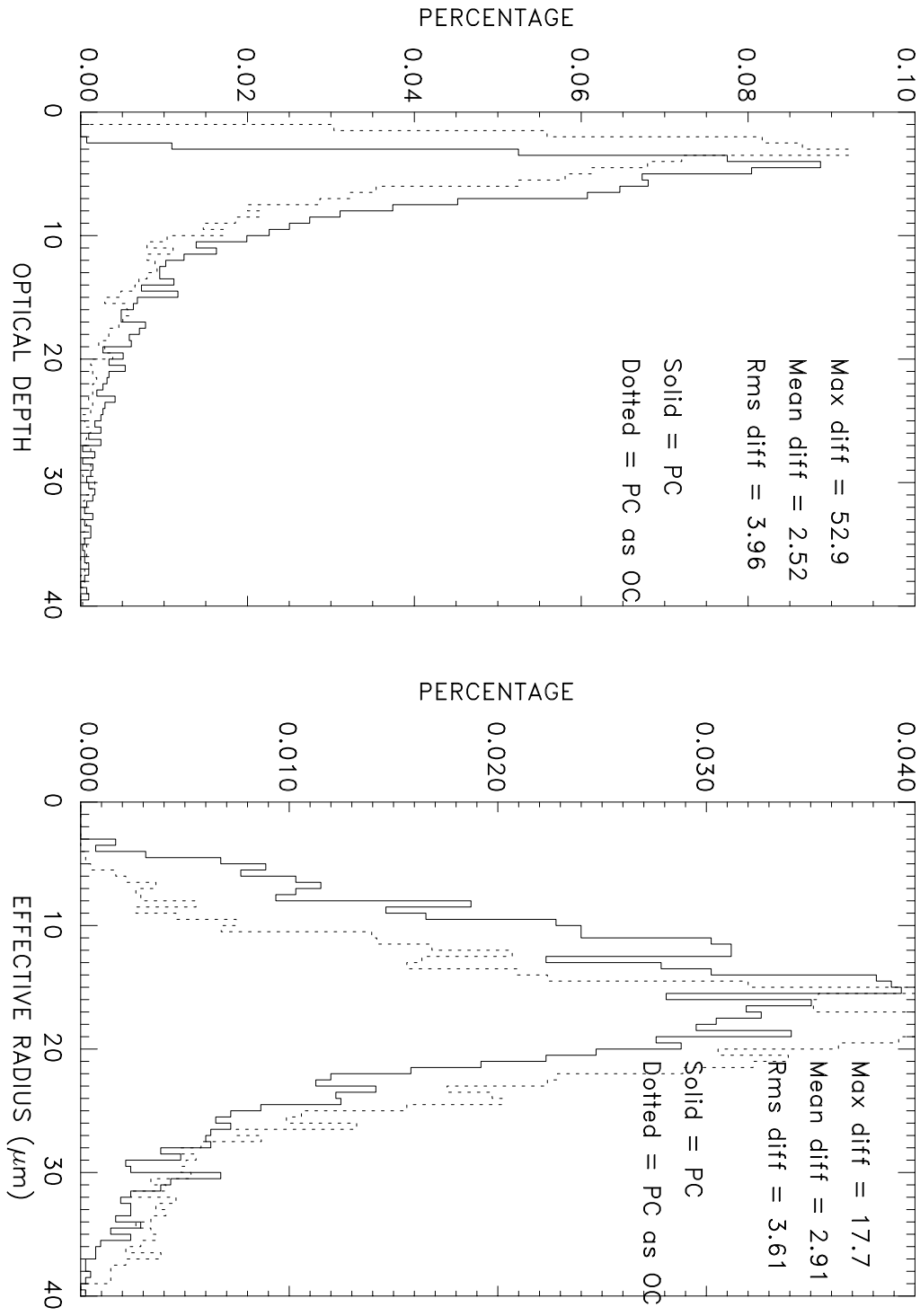

Partly cloudy pixels with cloud fractions greater than 0.20 were also retrieved assuming they were overcast and compared to the partly cloudy retrievals. The new "overcast" values for optical depth were slightly smaller than the partly cloudy retrievals. Effective radii retrievals were slightly larger than the partly cloudy retrievals.

PARTLY CLOUDY RETRIEVAL PRODUCTS

980222 19:57

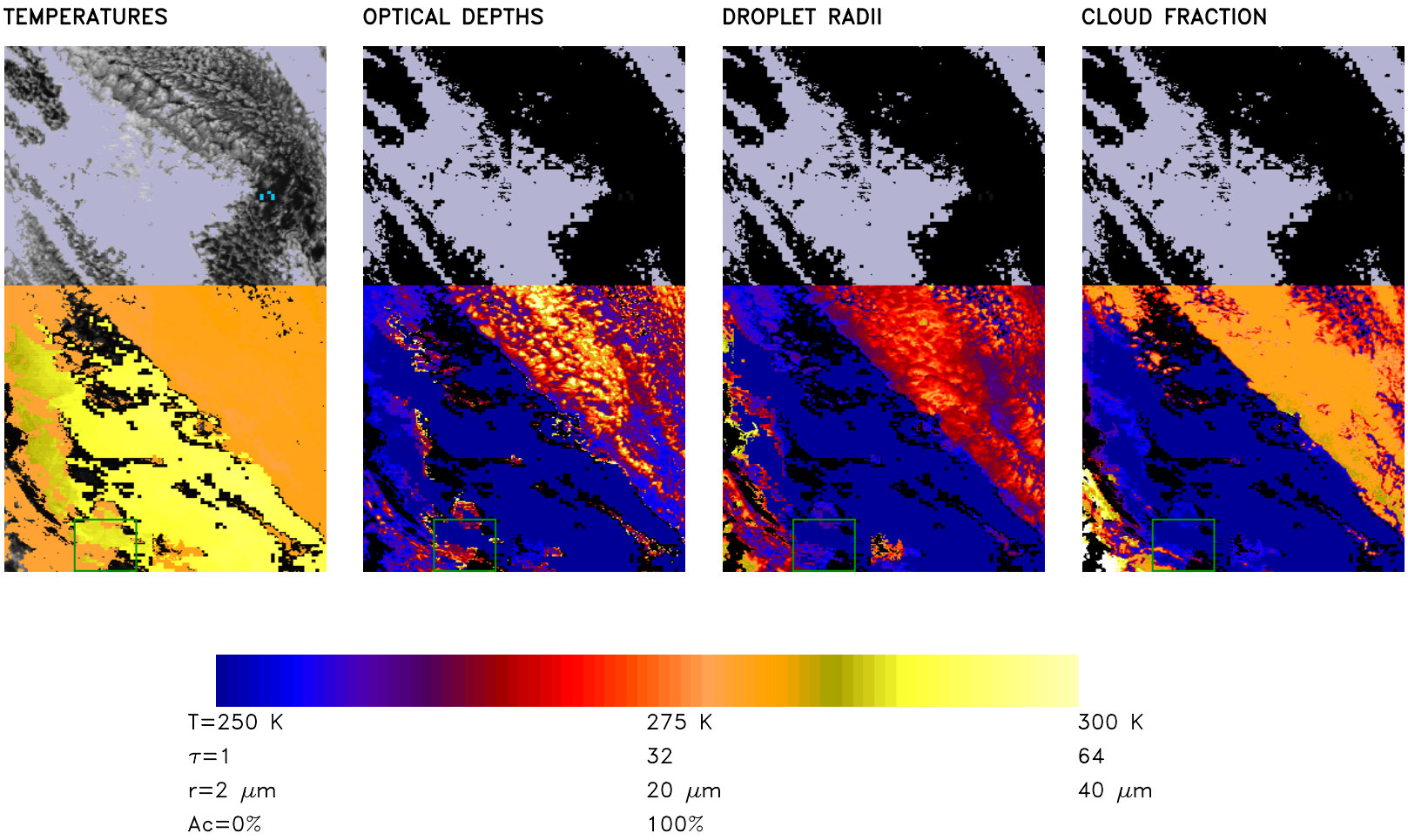

Partly cloudy retrieval products for another subregion were analyzed for a separate VIRS scene.

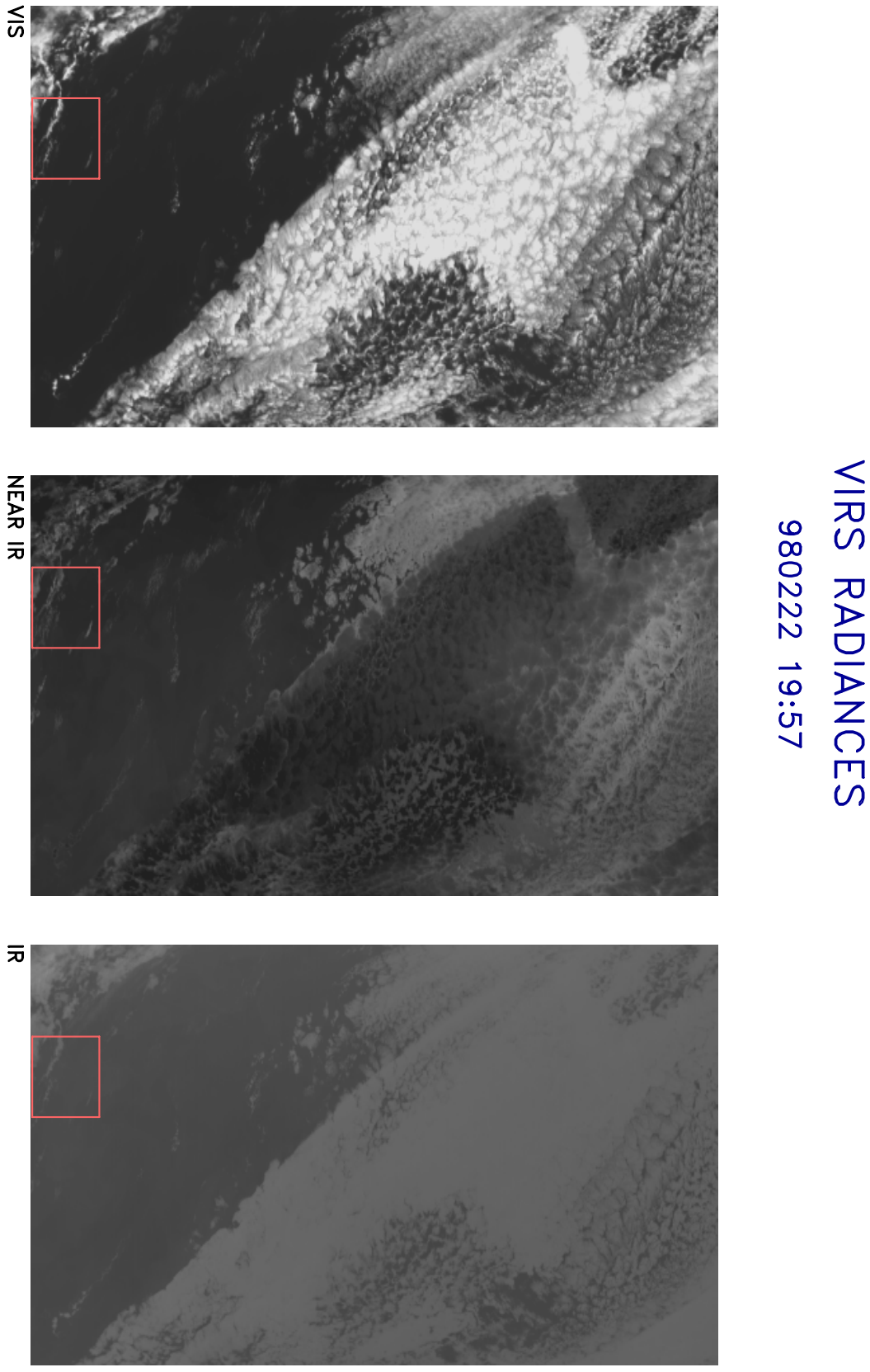

Corresponding pixel-level radiances are shown, with the analysis region outlined.

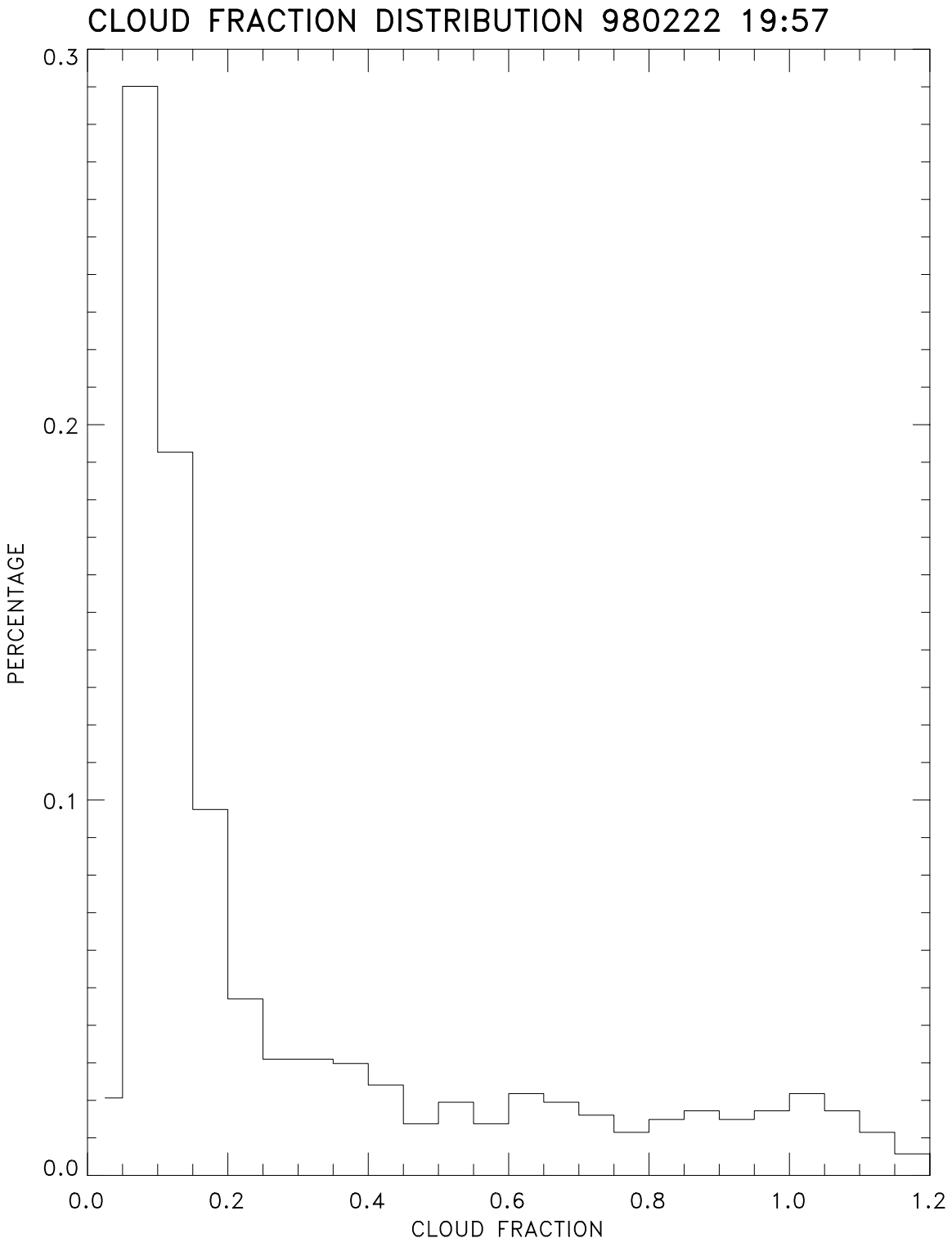

The cloud fraction distribution for this subregion is weighted toward lower cloud fractions, with most of the partly cloudy pixels having cloud fractions below 0.30.

PARTLY CLOUDY PROPERTIES 980222 19:57

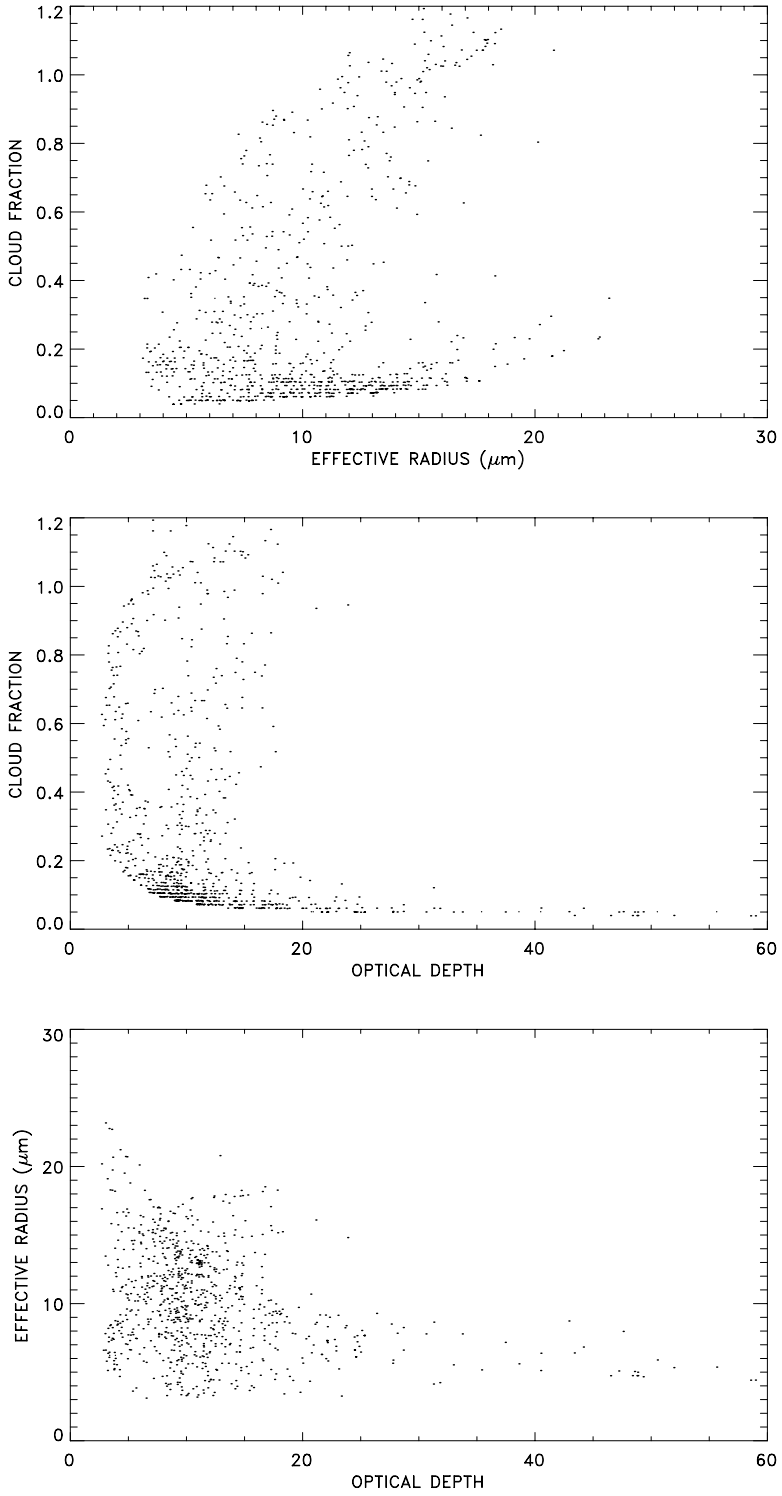

A weak dependence of retrieved effective radius for partly cloudy pixels on cloud fraction is evident for this subregion. The wide range of optical depths and effective radii at very small cloud fractions indicates the possible presence of surface reflection.

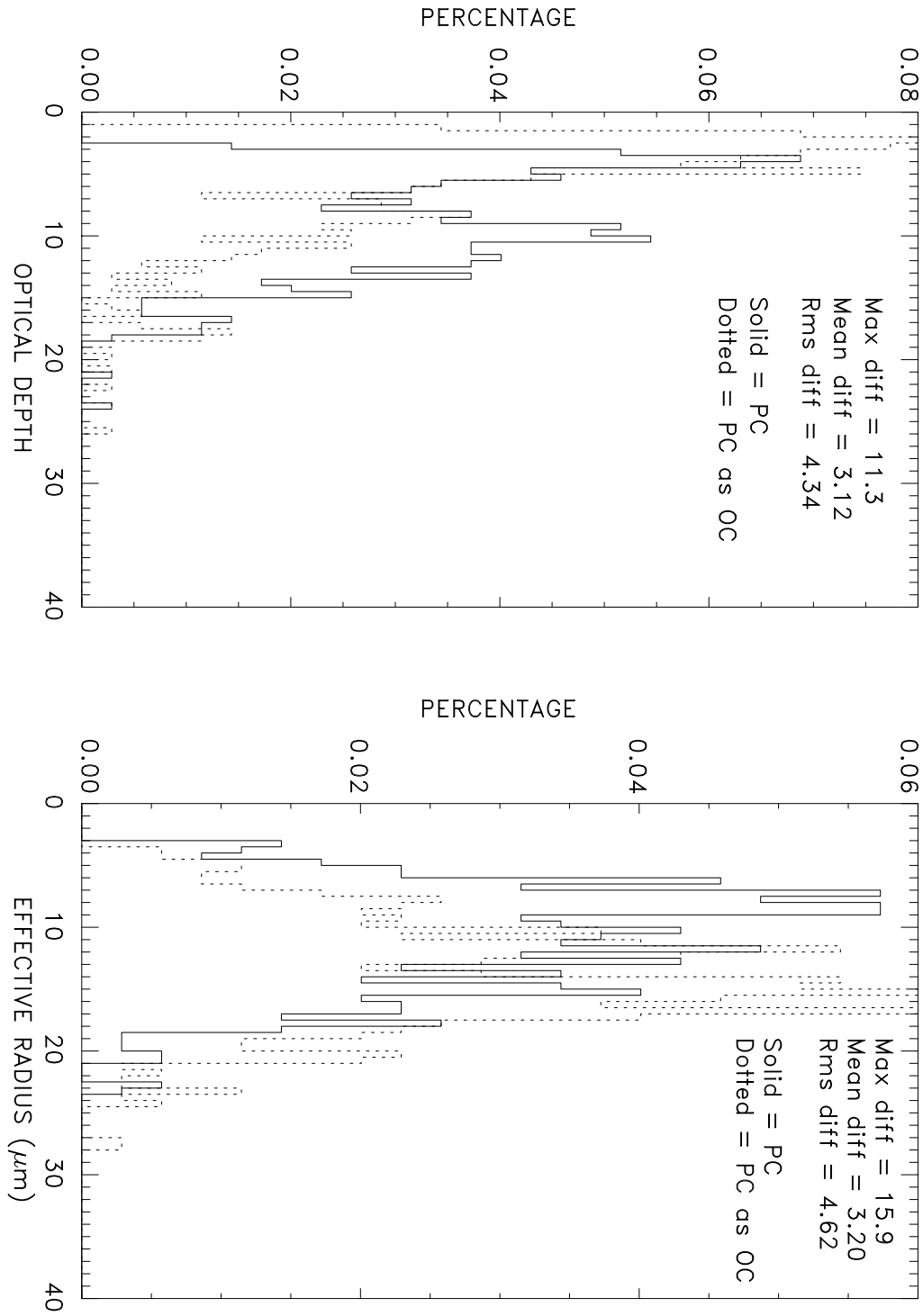

Partly cloudy pixels with cloud fractions greater than 0.20 were retrieved assuming they are overcast. The resulting optical depth values were slightly lower than the partly cloudy retrieval results. Effective radii retrievals with this assumption were slightly larger than the partly cloudy retrieval values.

Aerosol Radiative Forcing from CERES/TRMM and AERONET Data

By linking top of the atmosphere (TOA) radiative fluxes obtained by CERES/TRMM with surface measurements of aerosol optical depths obtained with the AERONET instrument at the Kaashidhoo Climate Observatory (KCO), Satheesh and Ramanathan (2000) derived emprical estimates of the direct aerosol radiative forcing for INDOEX. The proposal is to repeat their study for other oceanic AERONET sites. The approach will use an aerosol model to estimate the radiative forcing based on the CERES broadband radiance and the AERONET optical depth. The aerosol model is used to link the CERES radiance to a radiative flux and then to generate estimates of the diurnally averaged direct radiative forcing.

Satellite estimates of the aerosol direct radiative forcing made for INDOEX were found to be relatively insensitive to the aerosol model used to interpret the observed radiances. While some aerosol models gave rise to large errors in the retrieved optical depth, errors in the effect of the aerosol on the TOA radiative flux could be kept relatively small as long as the aerosol model used to retrieve the optical depth was also used to derive the radiative flux (Coakley et al. 2000).

The key to this compensation of errors is that for all sun-target-satellite viewing geometries the relationship between narrow-band and broadband reflectances is almost the same for aerosols with markedly different properties. For example, the NOAA Phase 1 aerosol, which is nonabsorbing and made up of small particles (Stowe et al. 1997), and the INDOEX First Field Phase (FFP) aerosol model, which is relatively strongly absorbing and has large particle components (Rajeev et al. 2000) produce nearly the same relationship. Differences in the TOA aerosol direct radiative forcing for INDOEX obtained using the NOAA Phase 1 and INDOEX FFP aerosol models differed by less than 30% even though the optical depths retrieved using these models differed by a factor of two (100%). This finding suggests that the selection of an aerosol model to deduce the TOA radiative forcing is not critical. Of course, the surface forcing, because it depends on the sunlight absorbed by the aerosol, will remain sensitive to the selection.

To verify that estimates of the TOA radiative forcing are relatively insensitive to the choice of the aerosol model, calculations of shortwave, broadband reflectances (0.2–4 μm) were performed using optical depths retrieved using VIRS reflectances associated with CERES fields of view designated as “Strong Clear” in the SSF. Optical depths were retrieved using the average continental and tropical marine aerosol models described by Hess et al. (1998). The models were used together in a 2-channel, 2-model retrieval scheme as well as separately in single-channel retrieval schemes. The calculated shortwave reflectances were compared with reflectances observed by the CERES radiometer. As commonly done in aerosol retrievals, the comparisons were restricted to viewing geometries away from regions of sun glint and in the direction of backscattered sunlight. Good agreement with CERES observations were obtained regardless of the retrieval method, aerosol model, and whether the scanner was operating in the cross track or rotating azimuth mode. For these comparisons, however, the best results were obtained by taking the ocean reflectance to be Lambertian with an albedo of zero.

While the approach described here was meant for SSF observations, the SSF were unavailable. Methods were explored for identifying ERBE-like cloud-free scenes suitable for aerosol radiative forcing estimates. The ratio of the standard deviation of the shortwave radiance to the mean of the shortwave radiance for ERBE-like clear sky ocean scenes within $1° \times 1°$ latitude-longitude regions was used as an index of cloud contamination. For a small sample of SSF data, ratios of less than 0.1 typically corresponded to clear sky fields of view of which 60% or more were also designated as Strong Clear. For larger values of the ratio, effects of cloud contamination in the ERBE-like clear sky fields of view were clearly evident.

For the $1° \times 1°$ latitude-longitude regions in which the shortwave radiances for the clear-sky fields of view met the criteria suitable for assessments of aerosol forcing, the shortwave radiance was used in conjunction with an aerosol model to derive an optical depth at a reference wavelength. This optical depth in turn was used to calculate a radiative flux. Instantaneous estimates of radiative fluxes were somewhat larger than the ERBE-like CERES fluxes by approximately 6%. Reasons for the differences have yet to be explored, but cloud contamination, the ocean reflectances used in the calculations of the radiative fluxes (Cox and Munk, 1954), and the anisotropic factors in the CERES inversion, as well as the fidelity of the radiative transfer model are potential sources of error.

The diurnally averaged TOA aerosol direct radiative forcing for KCO obtained with this approach is 36 Wm^{-2} per unit optical depth. The value obtained by Satheesh and Ramanathan (2000) for is 25 Wm^{-2} per unit optical depth. Similar analyses are planned for the other AERONET sites.

Measured and Retrieved 0.65-μm Optical Depths

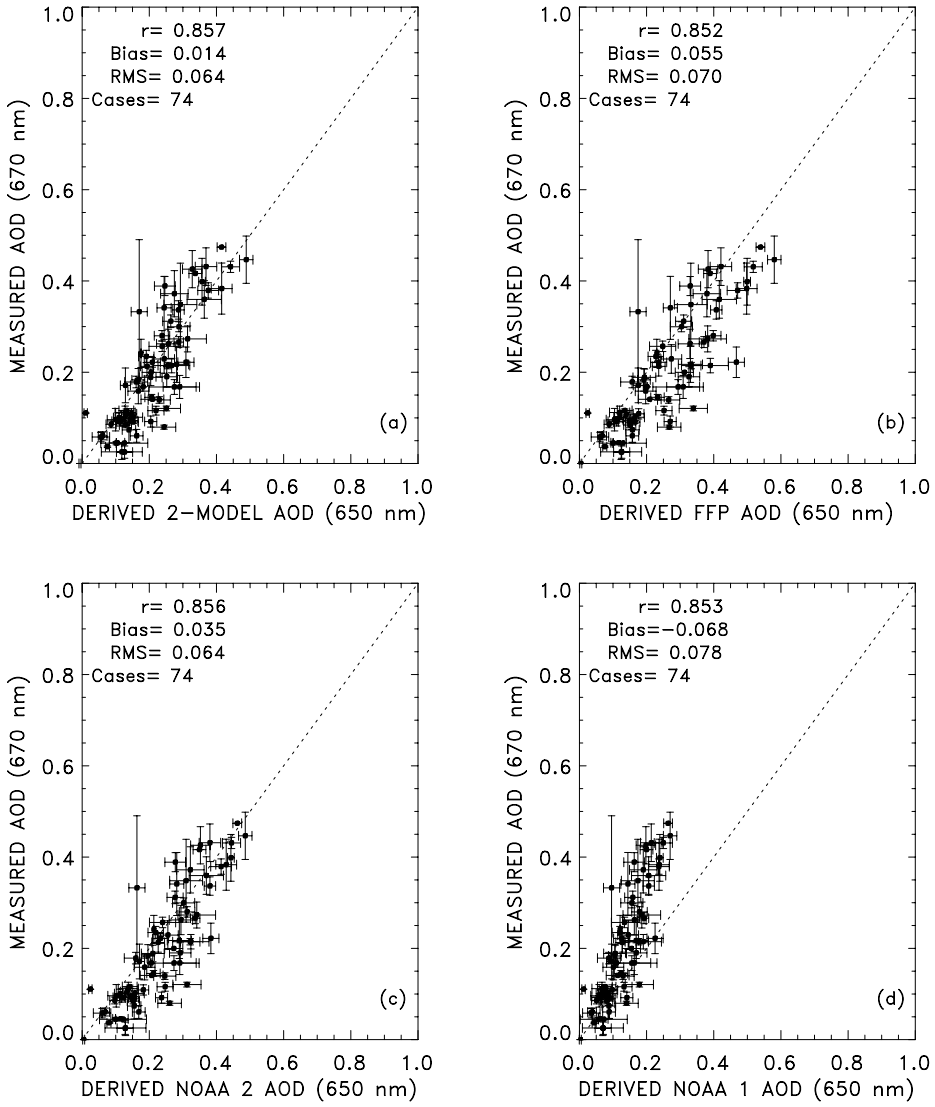

0.67-μm optical depths measured by surface and shipboard sun photometers and 0.65-μm optical depths retrieved using a) 2-channel, 2-model retrieval (Coakley et al. 2000); b) the INDOEX First Field Phase aerosol model in a single-channel retrieval (Rajeev et al. 2000); c) the NOAA Phase 1 and d) the NOAA Phase 2 retrievals (Stowe et al. 1997). Retrievals were performed using collocated (± 30 km), simultaneous (± 1 hr) reflectances measured with the NOAA-14 AVHRR. The observations include all matches for observations collected from January-March, 1996-2000. Error bars for the retrieved optical depths give the standard deviation for the fields of view that met the conditions for the retrieval. Error bars for the surface measurements give the standard deviation of the optical depths for the ± 1 hr period surrounding the satellite overpass.

Shortwave and Narrow-Channel Reflectances

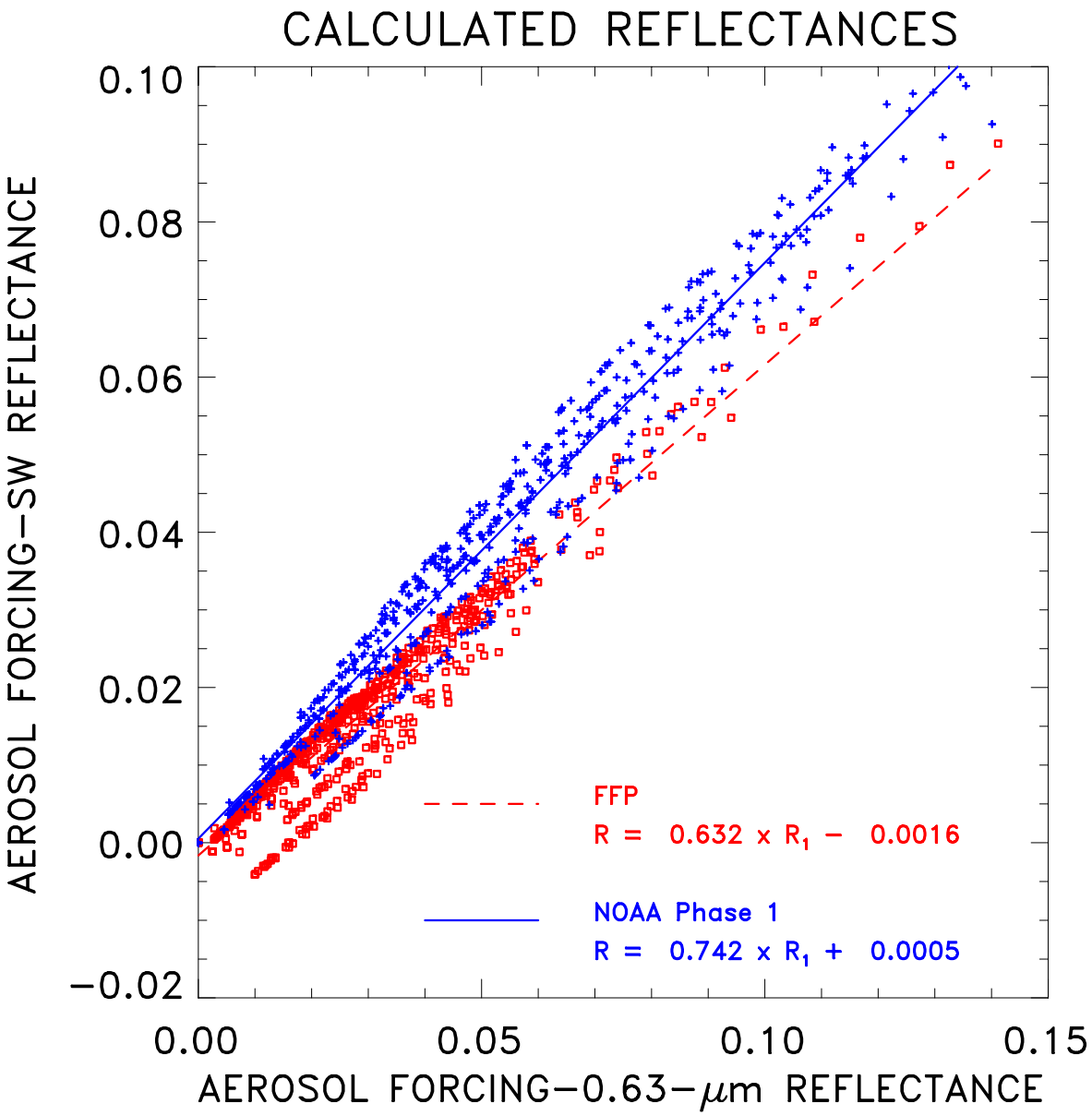

Shortwave (0.2–4 μm) and 0.63-μm cloud-free ocean reflectances for all sun-target-satellite viewing geometries outside of the sun glint domain for cases in which the 0.55-μm optical depths range from 0–0.9. Lines are linear least squares fits to the reflectances for the INDOEX First Field Phase aerosol model (Rajeev et al. 2000, dashed line, ?) and the NOAA Phase 1 model (Stowe et al. 1997, solid line, +).

Direct Aerosol Radiative Forcing

Cloud-Free Regions, February–March 1999

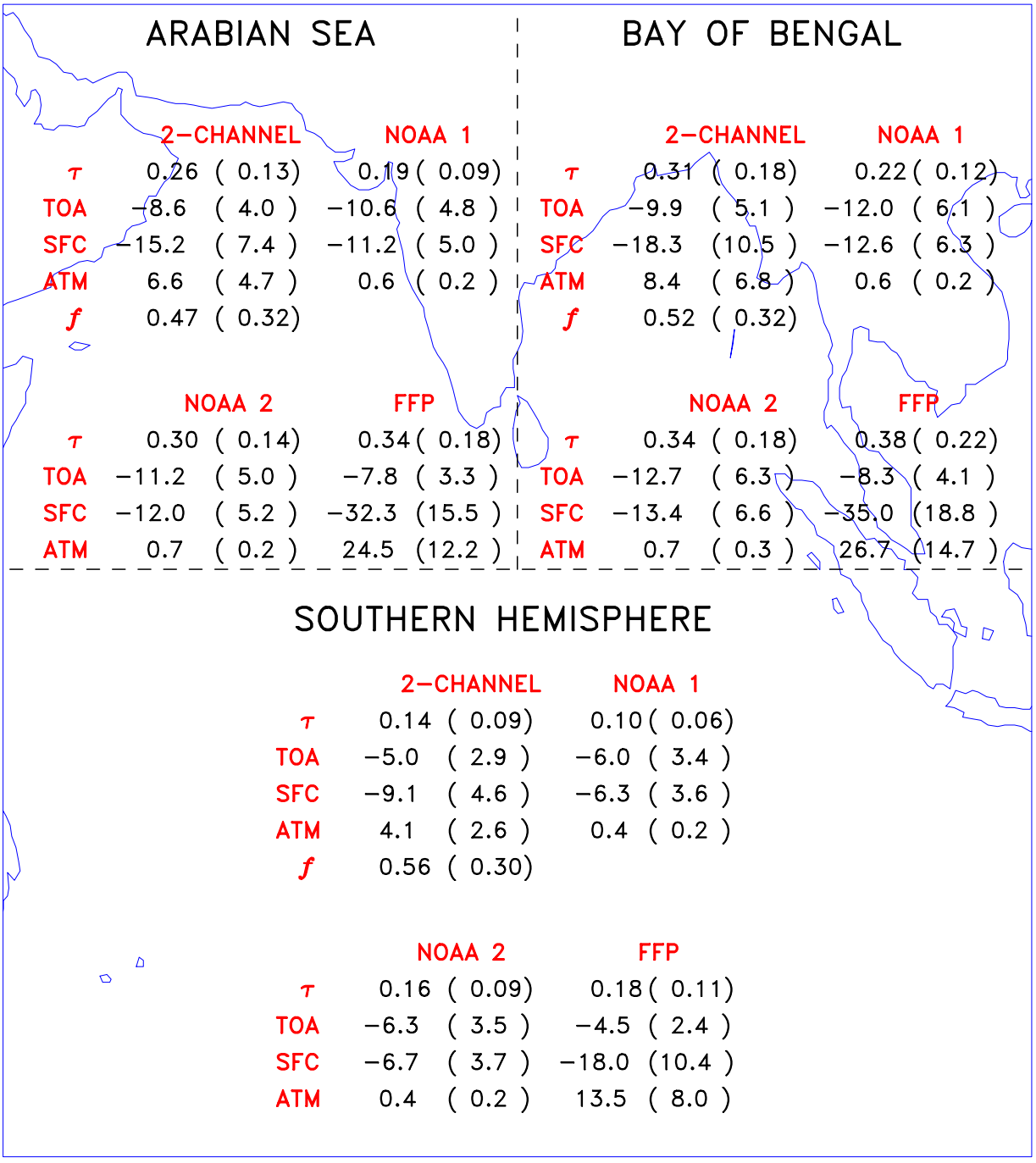

Cloud-free radiative forcing (Wm^{-2}) estimated using various retrieval schemes for determining aerosol properties (Coakley et al. 2000).

Observed and Calculated Broadband Shortwave Radiances

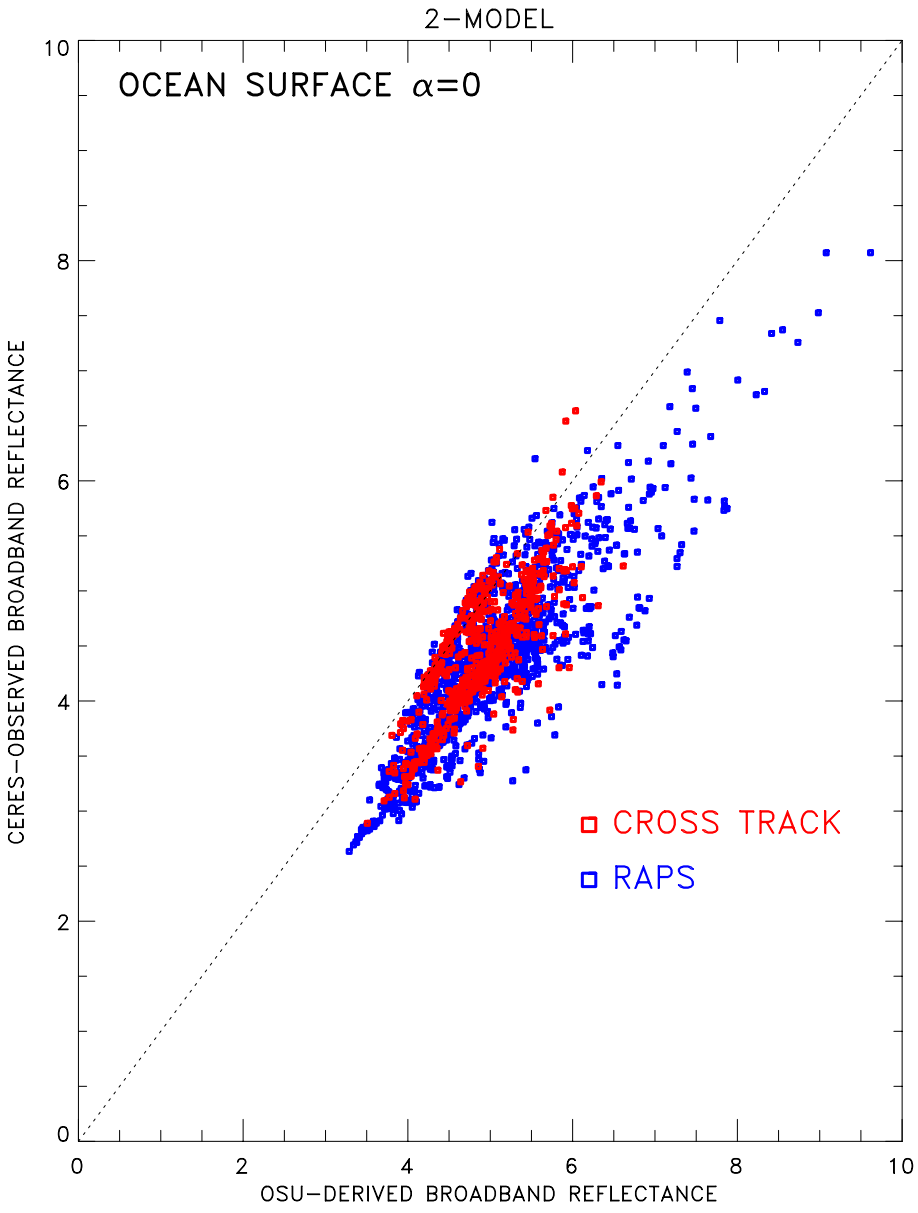

Shortwave radiances based on aerosol optical depths retrieved using VIRS reflectances for Strong Clear scenes in a 2-channel, 2-model retrieval scheme. Average continental and tropical marine aerosol models were used in the retrieval.

Observed and Calculated Broadband Shortwave Radiances

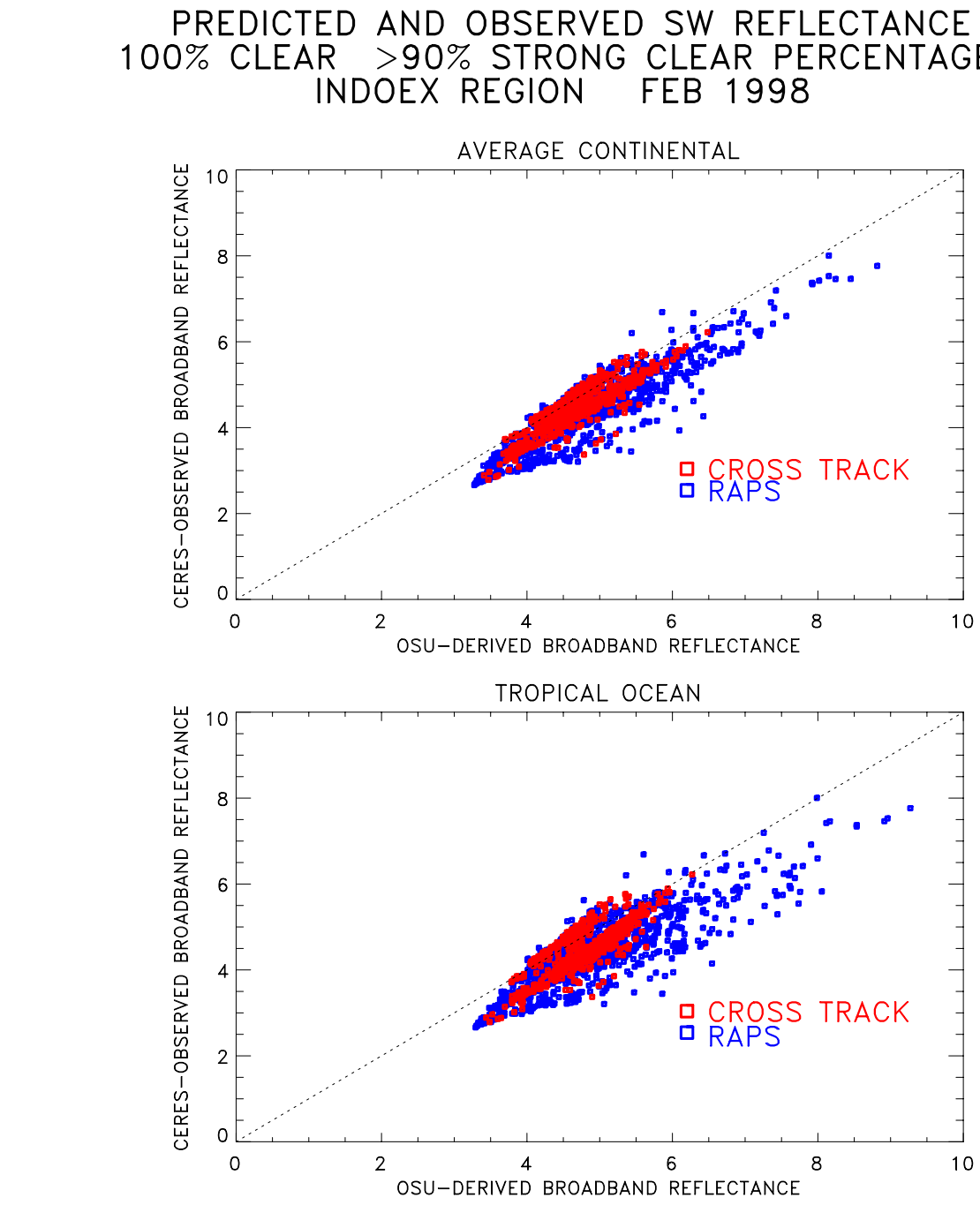

Shortwave radiances based on aerosol optical depths retrieved using VIRS reflectances for Strong Clear scenes in a single-channel, single-model retrieval scheme. Average continental and tropical marine aerosol models were used in the retrievals.

Strong Clear and ERBE Scene Type 1

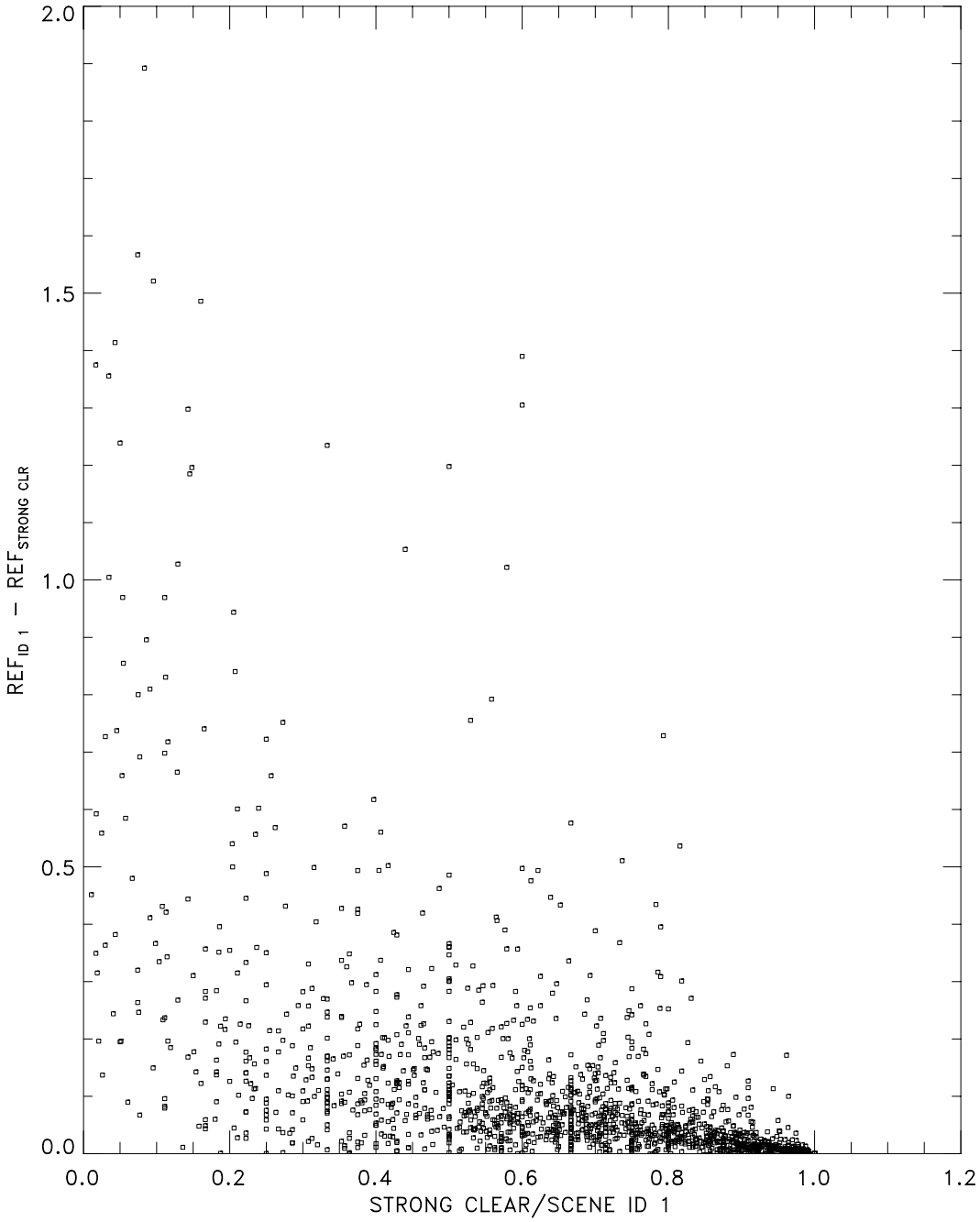

Difference in mean shortwave reflectances (ERBE Scene type 1 – Strong Clear) for 1° × 1° latitude-longitude regions and the fraction of the CERES fields of view identified as clear sky ocean that are also strong clear.

Spatial Uniformity as an Index of Strong Clear

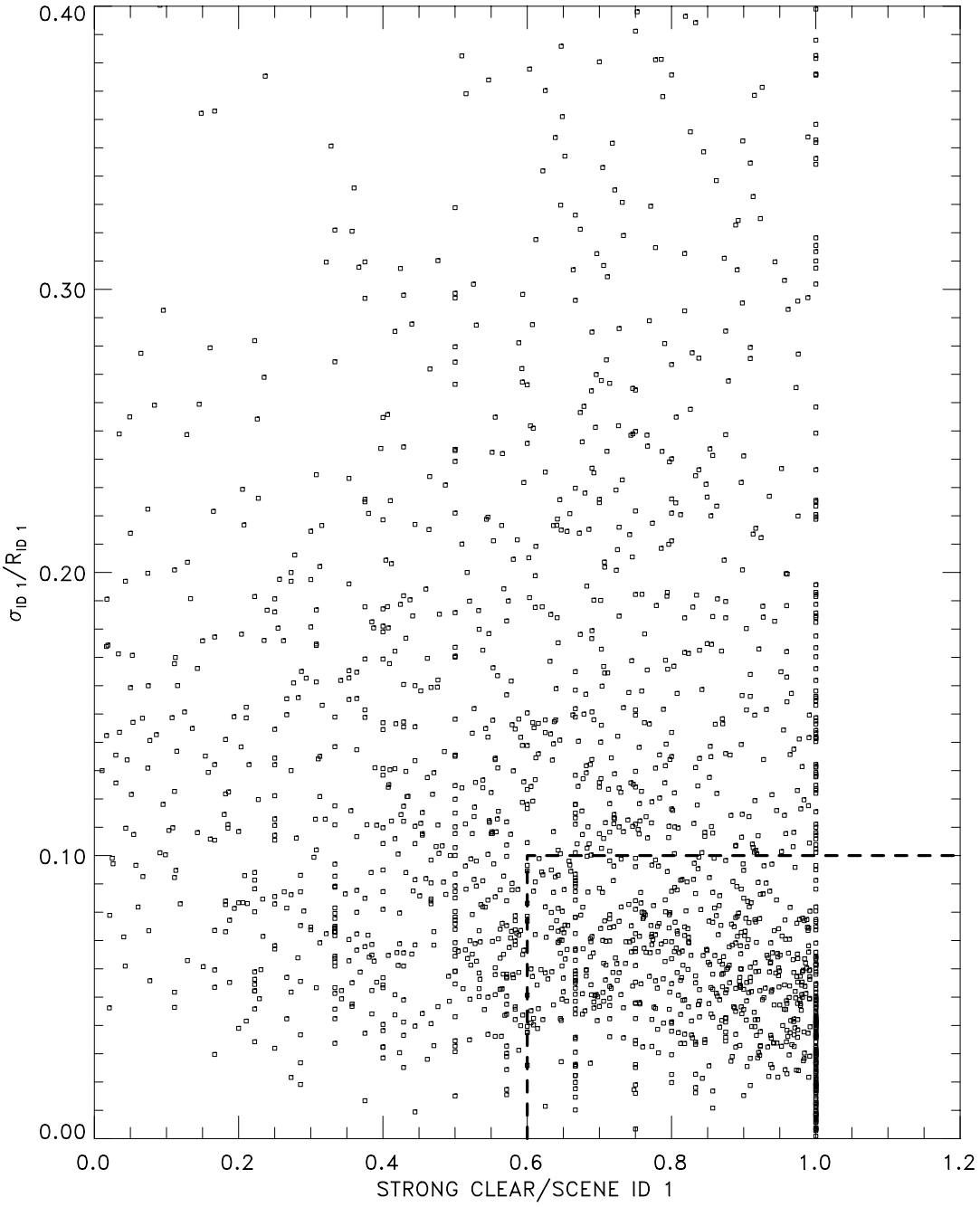

Ratio of the standard deviation of the shortwave reflectance to the mean reflectance for CERES fields of view identified as clear-sky ocean and the fraction of the fields of view identified as strong clear.

Modified Clear-Sky Ocean Identification

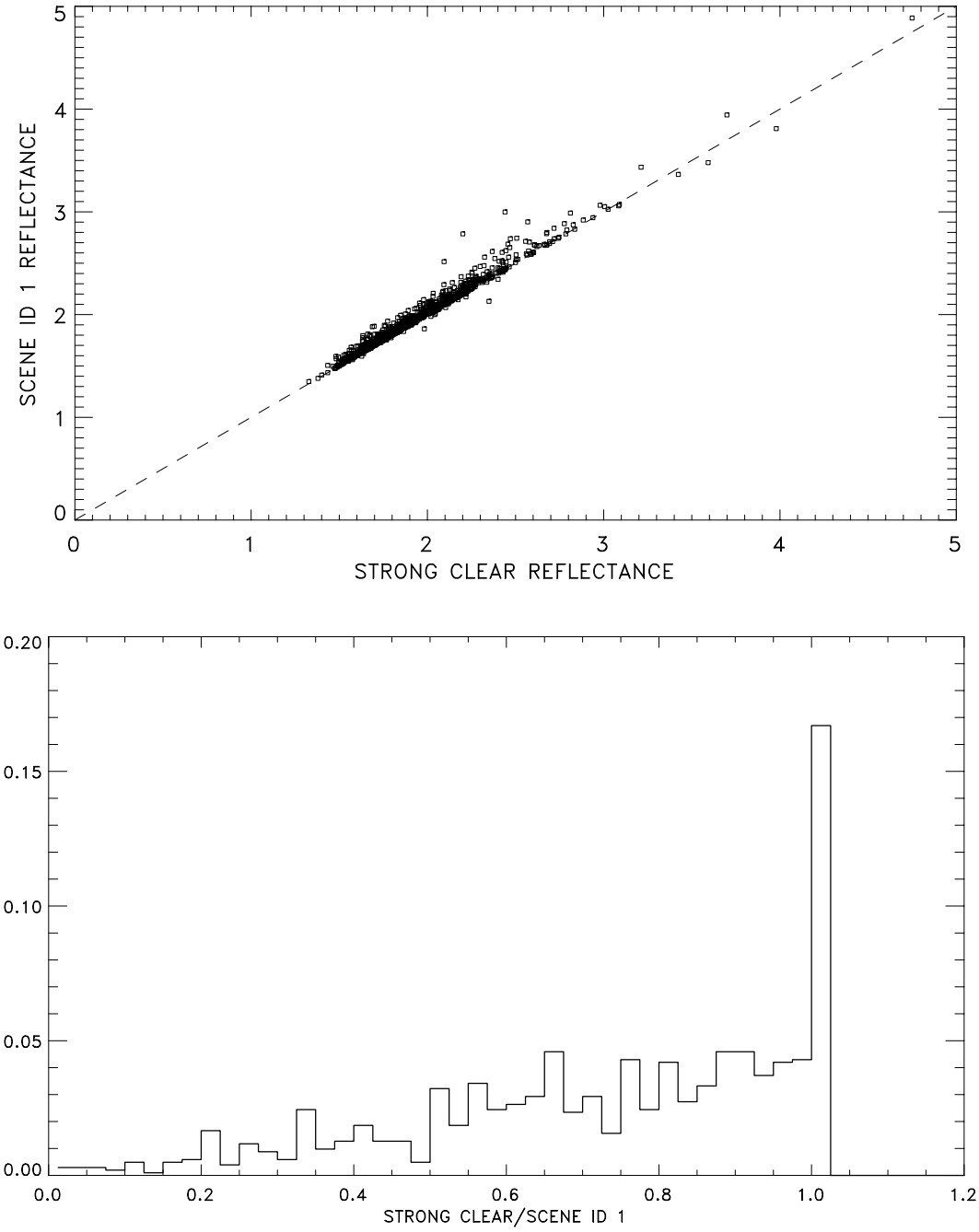

Shortwave radiances for clear sky ocean scenes for which the ratio of the standard deviation of the reflectance to the mean reflectance for 1° × 1° latitude-longitude regions is less than 0.1.

Reflected Shortwave Flux, KCO Comparisons

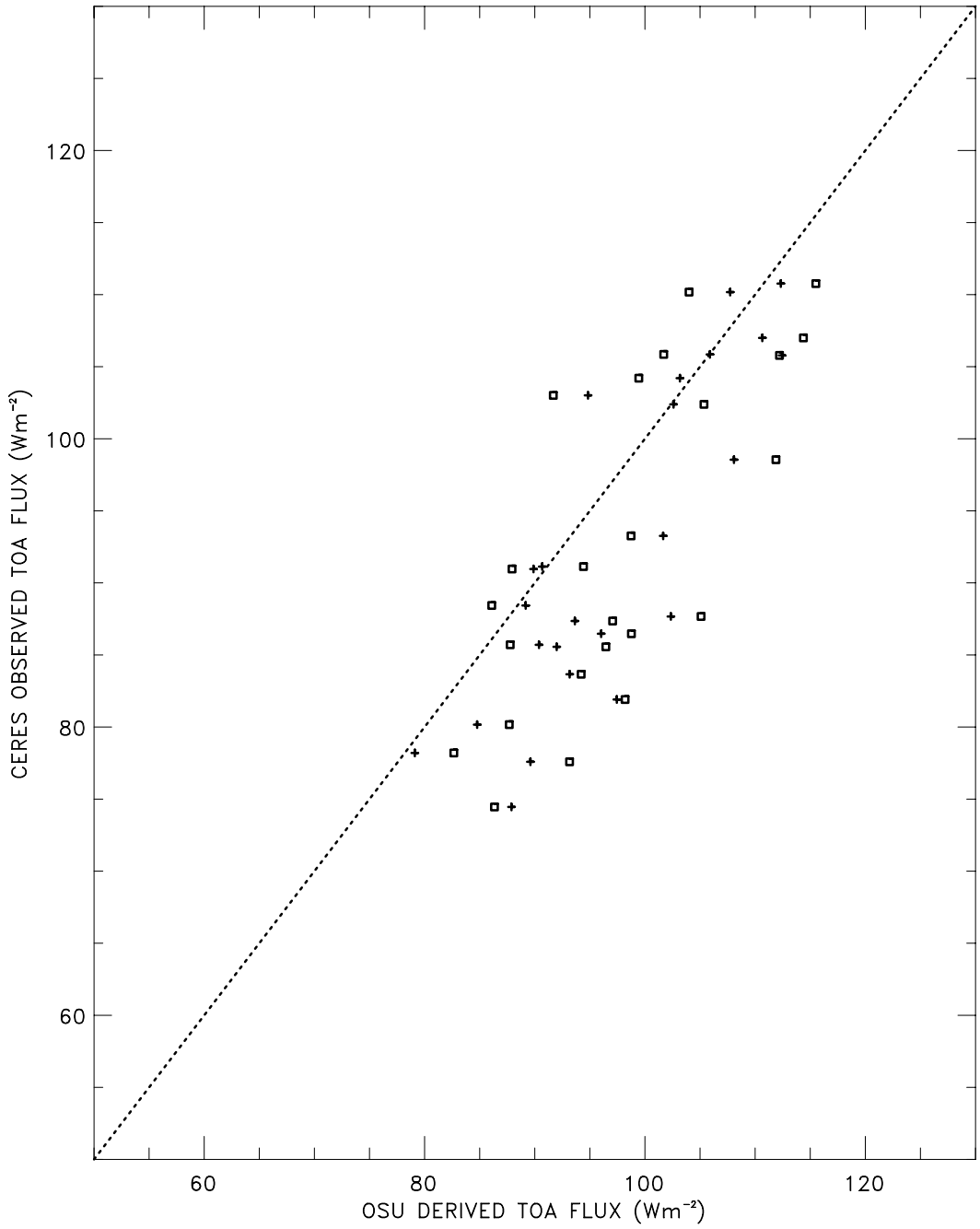

ERBE-Like (ES-8) and OSU-derived reflected shortwave fluxes for KCO when AERONET optical depths were available. Average continental (squares) and tropical marine aerosol models (crosses) were used to determine the radiative fluxes.

Diurnally Averaged, Clear-Sky Reflected Flux and Aerosol Optical Depth

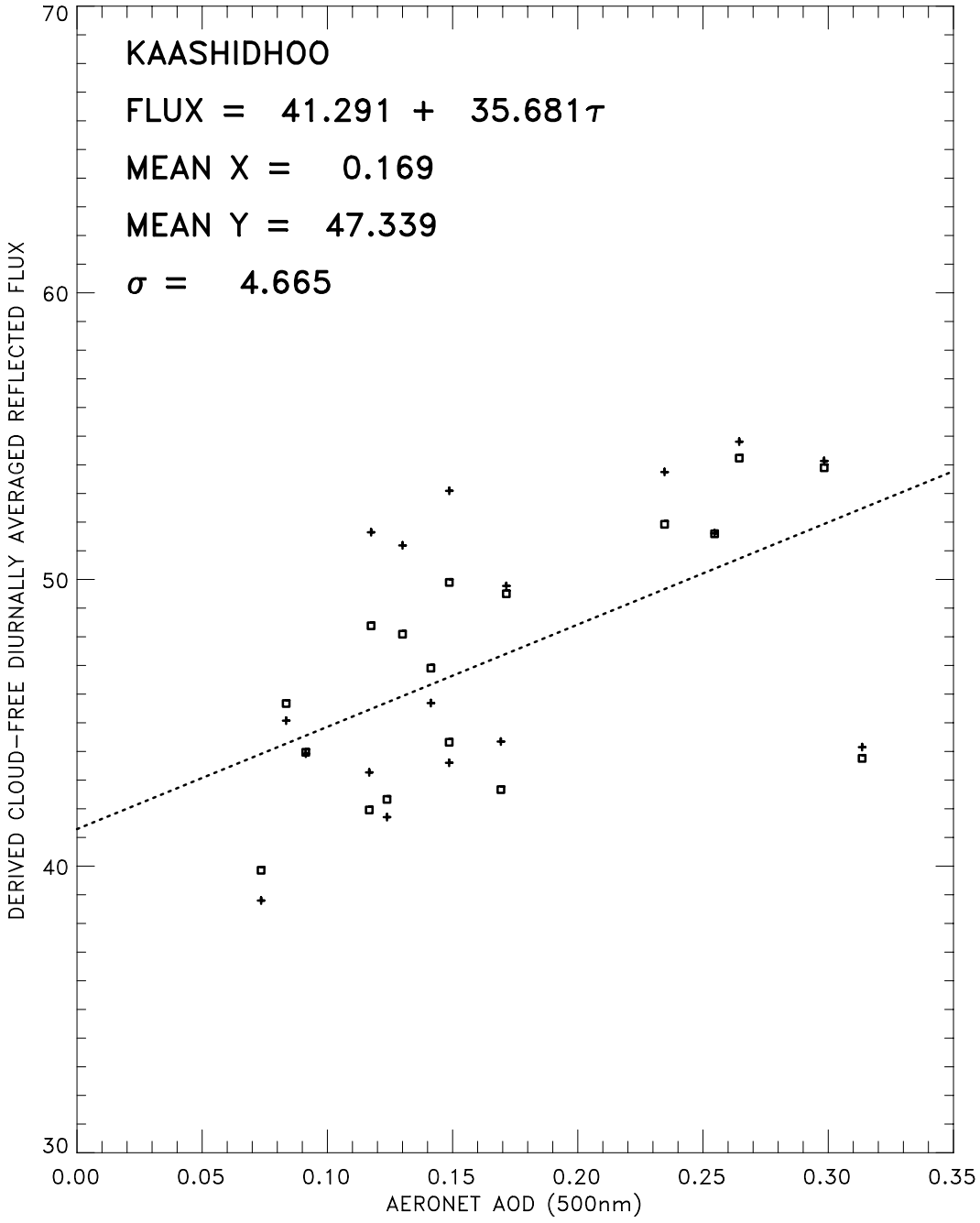

Diurnally averaged OSU-derived reflected flux and AERONET optical depths. The reflected fluxes were obtained using the average continental (squares) and tropical marine (crosses) aerosol models.

References

Coakley, J.A., Jr., W.R. Tahnk, A. Jayaraman, P.K. Quinn, C. Devaux, and D. Tanré, 2000: Aerosol Optical Depths and Direct Radiative Forcing for INDOEX Derived from AVHRR: Theory. *J. Geophys. Res*., (in preparation).

Cox, C., and W. Munk, 1954: Measurements of the roughness of the sea surface from the sun's glitter. *J. Opt. Soc. Am*., **44**, 838-850.

Hess, M., P. Koepke, and I. Schult, 1998: Optical properties of aerosols and clouds: The software package OPAC. *Bull. Amer. Meteor. Soc*. **79**, 831-844.

Kratz, D.P., 1995: The correlated k-distribution technique as applied to the AVHRR channels. *J. Quant. Spectrosc. Radiat. Transfer*, **53**, 501-517.

Rajeev, K., V. Ramanathan, and J. Meywerk, 2000: Regional aerosol distribution and its long-range transport over the Indian Ocean. *J. Geophys. Res.*, **105**, 2029-2043.

Satheesh, S.K. and V. Ramanathan, 2000: Large differences in tropical aerosol forcing at the top of the atmosphere and Earth's surface. *Nature*, **405**, 60-63.

Stamnes, K., S-Chee Tsay, W. Wiscombe, and K. Jayaweera, 1988: Numerically stable algorithm for discrete-ordinate-method radiative transfer in multiple scattering and emitting layered media. *Appl. Opt.*, **27**, 2502-2509.

Stowe,L.L., A.M. Ignatov, and R.R. Singh,. 1997: Development, validation, and potential enhancements to the second-generation operational aerosol product at the National Environmental Satellite, Data, and Information Service of the National Oceanic and Atmospheric Administration. *J. Geophys. Res*., **102**, 16,923-16,934.